

## COLOR-MAGNITUDE DIAGRAM CONSTRAINTS ON THE METALLICITIES, AGES, AND STAR FORMATION HISTORY OF THE STELLAR POPULATIONS IN THE CARINA DWARF SPHEROIDAL GALAXY

DON A. VANDENBERG<sup>1</sup>, PETER B. STETSON<sup>2</sup>, AND THOMAS M. BROWN<sup>3</sup>

*Submitted to The Astrophysical Journal*

### ABSTRACT

Victoria-Regina isochrones for  $-0.4 \leq [\alpha/\text{Fe}] \leq +0.4$  and a wide range in  $[\text{Fe}/\text{H}]$ , along with complementary zero-age horizontal branch (ZAHB) loci, have been applied to the color-magnitude diagram (CMD) of Carina. The color transformations that we have used have been “calibrated” so that isochrones provide excellent fits to the  $[(B-V)_0, M_V]$ -diagrams of M 3 and M 92, when well supported estimates of the globular cluster (GC) reddenings and metallicities are assumed. The adopted distance moduli, for both the GCs and Carina, are based on our ZAHB models, which are able to reproduce the old HB component (as well as the luminosity of the HB clump) of the dwarf spheroidal galaxy quite well — even if it spans a range in  $[\text{Fe}/\text{H}]$  of  $\sim 1.5$  dex, *provided* that  $[\alpha/\text{Fe}]$  varies with  $[\text{Fe}/\text{H}]$  in approximately the way that has been derived spectroscopically. Ages derived here agree reasonably well with those found previously for the old and intermediate-age turnoff stars, as well as for the period of negligible star formation (SF) activity ( $\sim 6$ – $10$  Gyr ago). CMD simulations have been carried out for the faintest turnoff and subgiant stars. They indicate a clear preference for SF that lasted several Gyr instead of a short burst, with some indication that ages decrease with increasing  $[\text{Fe}/\text{H}]$ . In general, stellar models that assume spectroscopic metallicities provide satisfactory fits to the observations, including the thin giant branch of Carina, though higher oxygen abundances than those implied by the adopted values of  $[\alpha/\text{Fe}]$  would have favorable consequences.

*Subject headings:* galaxies: abundances — galaxies: dwarf — galaxies: individual (Carina) — galaxies: stellar content — globular clusters: individual (M 3, M 92) — stars: evolution

### 1. INTRODUCTION

The color-magnitude diagram (CMD) of the Carina dwarf spheroidal (dSph) galaxy has three prominent features that set it apart from those of similar systems. The first, and perhaps most conspicuous, characteristic is the remarkable dichotomy of the horizontal branch (HB) into an intermediate-age, open-cluster-like red clump and an old, metal-poor, globular-cluster-like HB (see, e.g., Smecker-Hane et al. 1994, Hurley-Keller et al. 1998). In addition, deep photometric studies by Bono et al. (2010), Battaglia et al. (2012), and de Boer et al. (2014b), among others, have established that Carina has a very thin red-giant branch (RGB), despite the presence of stars that span a range in  $[\text{Fe}/\text{H}]$  from  $\sim -2.9$  to  $\sim -1.1$  according to the spectroscopic surveys carried out by, e.g., Shetrone et al. (2003), Koch et al. (2008), Lemasle et al. (2012), and Venn et al. (2012). Finally, the former investigations have shown that there is a clear gap in the distribution of stars on the subgiant branch (SGB) that separate the oldest ( $> 10$  Gyr) and intermediate-age ( $\lesssim 7$  Gyr) stellar populations, and possibly on the main sequence (MS) at  $V \sim 22.5$ ,  $B-V \sim 0.12$  between stars with ages  $\lesssim 2$  Gyr and those with higher ages. The evidence that Carina has undergone at least two distinct, well-separated star formation events over its evolutionary history seems undeniable.

Because Carina is so distant ( $\gtrsim 105$  kpc; e.g., Vivas & Mateo 2013), high-resolution spectra have been obtained for relatively few of its stars, despite the very considerable effort that has been made by several groups (including those mentioned

above). As a consequence, the trends of  $[m/\text{Fe}]$  with  $[\text{Fe}/\text{H}]$  (for individual metals  $m$ ) are not yet as well defined as they need to be in order for us to achieve a satisfactory understanding of Carina’s star formation history (SFH), and of its chemical evolution over time. Nevertheless, the available spectroscopic results suggest that the lowest metallicity stars in Carina have values of  $[\alpha/\text{Fe}] \approx +0.4$ , as typically found in Milky Way halo stars (e.g., McWilliam 1997). However, in contrast with the Galaxy, where such enhancements are characteristic of most stars with  $[\text{Fe}/\text{H}] \lesssim -1.0$ , the transition to low values of  $[\alpha/\text{Fe}]$  generally occurs at much lower iron abundances in dSph galaxies (see, e.g., Venn et al. 2004, Kirby et al. 2011). This is usually attributed to low star formation rates in the latter (e.g., Gilmore & Wyse 1998), which would have the consequence that Type Ia supernovae (SN) could begin to contribute to their chemical evolution before the gas had been enriched to very high  $[\text{Fe}/\text{H}]$  values by exploding massive stars.

In the case of the oldest Carina stars, the “knee” in the  $[\alpha/\text{Fe}]$  vs.  $[\text{Fe}/\text{H}]$  relationship appears to occur at  $[\text{Fe}/\text{H}] \sim -2.6$  (de Boer et al. 2014a), where the plateau at lower metallicities changes into a roughly linear decrease of  $[\alpha/\text{Fe}]$  to subsolar values at  $[\text{Fe}/\text{H}] \gtrsim -1.4$ . (Where this sequence terminates is not entirely clear due to the small numbers of observed stars and the considerable scatter in the derived abundances; also see de Boer et al. 2014b.) Regardless, because the intermediate-age (IA) population includes stars that formed with  $[\text{Fe}/\text{H}] \sim -1.8$  and  $[\alpha/\text{Fe}] \approx +0.4$ , while the oldest population contains some stars at higher  $[\text{Fe}/\text{H}]$ , it is clear that Carina has undergone inhomogeneous chemical evolution (Venn et al. 2012). This could plausibly be explained by gas infall (see the discussions by Lemasle et al. 2012 and de Boer et al. 2014b). (It is a reasonable expectation that each major SF event would produce an increase in  $[\alpha/\text{Fe}]$  — but not necessarily to same value that is found in the preceding gen-

<sup>1</sup> Department of Physics & Astronomy, University of Victoria, P.O. Box 1700, STN CSC, Victoria, BC, V8W 2Y2, Canada; vandenberg@uvic.ca

<sup>2</sup> Herzberg Institute of Astrophysics, National Research Council of Canada, 5071 West Saanich Road, Victoria, BC, V9E 2E7, Canada

<sup>3</sup> Space Telescope Science Institute, 3700 San Martin Drive, Baltimore, MD 21218, USA; tbrown@stsci.edu

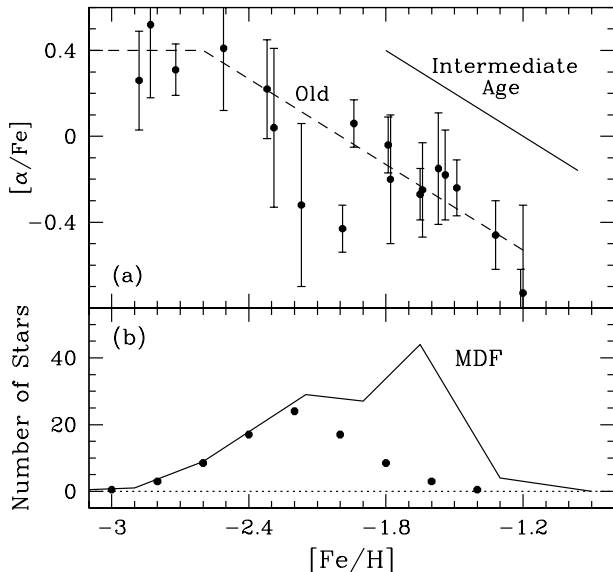


**Figure 1.** *Panel (a):* approximate mean  $[\alpha/\text{Fe}]$  versus  $[\text{Fe}/\text{H}]$  relations for the oldest and intermediate-age stellar populations of Carina (the dashed and solid curves, respectively). The dashed curve, which reproduces the results given by de Boer et al. (2014a; their Fig. 3), clearly provides a good fit to the spectroscopic abundances compiled by Lemasle et al. (2012; see their Table 10), assuming that  $[\alpha/\text{Fe}] = [\text{Mg}/\text{Fe}]$  (see the text). The solid curve is suggested by a plot of the same data that was published by Venn et al. (2012, their Fig. 20). Only those stars in the Lemasle et al. sample that have significantly different iron and Mg, and hence  $\alpha$ -element, abundances relative to the values along the solid curve have been plotted (the filled circles with attached vertical error bars) because we are mainly interested in the “Old” stars. *Panel (b):* schematic reproduction of the Carina MDF that was derived by Starkenburg et al. (2010). The filled circles depict the variation in the number of stars with  $[\text{Fe}/\text{H}]$  that has been adopted in this study for the oldest Carina stars (those having chemical properties represented by the dashed curve) in the upper panel.

eration — which subsequently falls with increasing  $[\text{Fe}/\text{H}]$  as the SF rate declines; see Gilmore & Wyse 1991.)

Based on the Mg abundances reported by Lemasle et al. (2012, also see Venn et al. 2012), the Mg/Fe number abundance ratios in stars belonging to the IA population appear to decrease from  $[\text{Mg}/\text{Fe}] \approx +0.4$  at  $[\text{Fe}/\text{H}] \sim -1.8$  to  $\approx 0.0$  at  $[\text{Fe}/\text{H}] \sim -1.2$  (but with a large scatter, mostly to very low values of  $[\text{Mg}/\text{Fe}]$ ). The same studies show that calcium abundances are considerably more uniform, suggesting no more than a shallow slope in the  $[\text{Ca}/\text{Fe}]$  vs.  $[\text{Fe}/\text{H}]$  relation over the same range in iron content. Because magnesium has a far bigger impact on stellar models due to its much greater absolute abundance (see VandenBerg et al. 2012, hereafter V12), Mg is arguably a better tracer of  $[\alpha/\text{Fe}]$  than Ca. For this reason and the above considerations, we have adopted the relations between  $[\alpha/\text{Fe}]$  and  $[\text{Fe}/\text{H}]$  for the oldest and IA populations of Carina that are shown in Figure 1a. The abundances for individual stars have been plotted only if they have  $[\text{Fe}/\text{H}] < -1.8$  or they have  $[\text{Mg}/\text{Fe}]$  values that differ by more than 0.25 dex, at their  $[\text{Fe}/\text{H}]$  values, from those indicated by the solid curve. These data suggest that the dashed locus probably does extend to  $[\text{Fe}/\text{H}] \sim -1.2$  (but see de Boer et al. 2014b). Furthermore, the observed large scatter in the Mg, and hence  $\alpha$ -element, abundances at  $[\text{Fe}/\text{H}] \gtrsim -1.8$  is a natural outcome if stars with these iron abundances lie along two, well-separated  $[\alpha/\text{Fe}]$  versus  $[\text{Fe}/\text{H}]$  relations.

The Carina metallicity distribution function (MDF) that was derived by Starkenburg et al. (2010), on the basis of their improved calibration of Ca II triplet absorption line strengths

in terms of  $[\text{Fe}/\text{H}]$ , is given in Fig. 1b. Most of the stars in Carina have  $[\text{Fe}/\text{H}]$  values between  $\sim -2.8$  and  $-1.3$ , with just a few stars at both lower and higher metallicities. Local peaks in the number count distributions occur at  $[\text{Fe}/\text{H}] \approx -2.2$  and  $-1.65$ . Although based on a much smaller sample, the MDF derived more recently by Lemasle et al. (2012) agrees quite well with the Starkenburg et al. findings. The main difference between them is at  $[\text{Fe}/\text{H}] \sim -2.0$ , where significantly fewer stars, relative to the peaks on either side, are present in the Lemasle et al. sample.

Insofar as ages are concerned, the narrow RGB of Carina together with the lack of any obvious metallicity dependence of the colors of red giants at a common luminosity implies that ages and metallicities are anti-correlated (see, e.g., Koch et al. 2006).<sup>4</sup> Although there have been some attempts to determine the ages of bright giants using isochrones so close to the spectroscopically derived  $[\text{Fe}/\text{H}]$  values (e.g., Lemasle et al. 2012), “the small offset in color with age ... combined with the sensitivity to the largely unknown elemental abundance mix and He content limits the usefulness of this exercise” (Koch et al. 2006). Any dispersion in the observed abundances of the  $\alpha$ -elements at the same  $[\text{Fe}/\text{H}]$  will have important consequences for the effective temperatures (and presumably the colors) of red giants, at a fixed age (as shown by V12). Ages are much more reliably determined for turnoff (TO) and SGB stars since, at low metallicities, TO luminosity vs. age relations depend almost entirely on the absolute abundance of oxygen (and of C and N); the other metals mainly affect the predicted  $T_{\text{eff}}$  scale in a relatively minor way (see V12). Unfortunately, as noted by Monelli et al. (2014), very little is known about the abundances of the CNO elements, and their variations with  $[\text{Fe}/\text{H}]$ , in this (or any other) dSph galaxy.

When this project began (in mid-2014), it was our intention to use the latest Victoria-Regina isochrones (VandenBerg et al. 2014a; hereafter V14a) for  $-0.4 \leq [\alpha/\text{Fe}] \leq +0.4$  (and a wide range in  $[\text{Fe}/\text{H}]$ ), together with new, complementary color transformations (Casagrande & VandenBerg 2014, hereafter CV14), to study the implications of the very narrow RGB of Carina, and to try to shed some light on a possible conflict between photometrically inferred and spectroscopically derived metallicities. A few years earlier, Bono et al. (2010; also see Lianou et al. 2011) had concluded, mainly from the superposition of Galactic star cluster fiducial sequences onto the Carina CMD and theoretical simulations of the latter, that the spreads in  $[\text{Fe}/\text{H}]$  encompassed by both the oldest and the intermediate-age (IA) populations in the dSph galaxy appear to be considerably less than those derived from spectroscopic data (also see Fabrizio et al. 2012).

However, there is a third motivation for the present undertaking. When interpreting the photometry of complex stellar populations (as in the case of Carina), it is important to check that the isochrones which are used to determine their properties (e.g., ages, SFH) faithfully reproduce the CMDs of simple(r) systems, like globular clusters (GCs). If they fail to do so, they cannot be expected to overlie stars in galactic CMDs that have the same age and chemical abundances, but different evolutionary states (due to differences in mass). In fact, it is a

<sup>4</sup> Only recently has it been possible to separate the most metal-poor giants from those having intermediate metallicities using measurements of the  $c_{U,B,I} = (U-B) - (B-I)$  index (Monelli et al. 2014). However, as discussed in the latter study, it has proven to be difficult to explain such observations using current isochrones, perhaps because the assumed heavy-element mixtures are not representative of the actual stellar abundances.

good idea to “calibrate” stellar models using GCs and/or open clusters before applying them to complicated systems — as in the study of Andromeda’s SFH by Brown et al. (2006) and their recent analyses of the CMDs for several ultra-faint dwarf (UFD) galaxies (Brown et al. 2014, 2012). This has generally not been done in studies of Carina, but we have opted to do so here. [Note that the ages of most star clusters are not subject to this concern because they can be derived by matching isochrones to just a small part of the CMD containing the turnoff luminosity (via, e.g., the procedure described by VandenBerg et al. 2013; hereafter V13). In the case of galaxies, ages are effectively determined on a star-by-star basis, and the isochrones which are used should provide good fits to photometric data in all of the evolutionary stages that are studied in order to obtain the most reliable results.]

The next section describes the observations that are employed in this investigation, both of Carina and of the GCs M3 and M92, which are used to calibrate the stellar models (see § 3) that have been applied to the CMD of the dSph (as reported in § 4). Because the most recent Victoria-Regina isochrones (V14a) are restricted to ages  $\gtrsim 5$  Gyr, the main focus of this project is on the faintest TO stars in Carina, which we have attempted to explain through the superposition of isochrones onto their observed CMD locations, as well as numerical simulations. The latter enable us to probe the SFH of Carina. A short summary of our findings is given in § 5.

## 2. PHOTOMETRY OF CARINA, M92, AND M3

The data for Carina discussed here are the same as those that were the subject of the analysis by Bono et al. (2010). They resulted from the analysis of more than 4,000 CCD images obtained during 27 observing runs between 1992 December and 2008 September. The observational indices from each observing run were transformed to the standard Johnson *UBV*, Kron-Cousins RI photometric magnitude system of Landolt (1992; supplemented by additional measurements in the *UBV* filters by Landolt 1973) following the procedures described by, e.g., Stetson (2000, 2005). Then the average results from all observing runs were used to define a network of local photometric standard stars in the Carina field, to which observations of all other stars in the field were referenced.

Exactly the same procedures were employed to produce the photometric results for our comparison clusters, M3 (= NGC 5272) and M92 (= NGC 6341). The results for these two clusters come from 21 observing runs (1984 June–2002 March) for M3 and 40 observing runs (1984 June–2002 May) for M92.

In the final analysis, these results are tied to 324 and 336 Landolt stars in the *B* and *V* filters, and 231 Landolt stars in the *I* filter. If we consider the *V* filter as representative, the median number of observations per star by Landolt is 16; the median number of observations per star by us is 69. We find that the r.m.s. dispersion of the difference between Landolt’s and our average photometric results is 0.012 mag per star in *B*, 0.009 mag in *V*, and 0.011 mag in *I*. We believe that this represents an irreducible limit to our ability to transform indices from one typical set of broad-band filters to another, given the inherent differences in the detailed spectral energy distributions of stars of a given perceived color. The net difference between Landolt’s overall photometric system and our attempt to reproduce that system should be of order 0.01 mag divided by the square root of a number of order a few hundred, at least within the range of temperature, gravity, and chemical abundance that is spanned by Landolt’s (mostly Population I)

photometric standards.

It is true that our photometric study of Carina requires that we apply transformations derived from field standard stars of mostly solar metallicity to program stars that are appreciably metal-poor. To the extent that different filter sets differently sample the stellar spectral-energy distributions, this could in principle introduce a systematic difference between the results of any one of our filter sets and Landolt’s filter set. Given that our 27 observing runs employed at least six different combinations of detector and filter set, this should mitigate any net systematic difference between the average photometric indices obtained by us and those that Landolt would have obtained by observing Carina with his equipment. In any case, if there does remain a metallicity-dependent difference between what we did measure and what Landolt would have measured, it should affect Carina, M3, and M92 similarly, and should be negligible in differential comparisons. We therefore believe that comparisons between our observations and our theoretical predictions will be more hampered by imperfect approximations in the theoretical modelling, by uncertain transformations between the theoretical and observational indices, and perhaps by imperfect knowledge of the reddening toward Carina, than by random or systematic errors in the photometry.

To select our samples of well-observed, probable members of each system, we first estimated the photometric barycenter of the target and then plotted the relationship between apparent magnitude and photometric uncertainty as a function of the radial distance of the star from the center of its host system. In particular, we plotted *V*-band magnitude versus radius for stars with  $0.01 < \sigma(B-I) < 0.02$  mag,  $0.04 < \sigma(B-I) < 0.06$  mag, and  $0.08 < \sigma(B-I) < 0.10$  mag. We then chose an annulus where all of these radial plots were essentially flat. Toward smaller radii the errors increase (or, more correctly stated, the apparent magnitude typical of a given photometric error becomes brighter) due to crowding; toward larger radii, the errors increase because those parts of the field typically appear in fewer CCD images. As a further limit on the outer radius of the annulus we plotted observed color versus radius for stars within a small apparent magnitude range around the cluster turnoff. We made sure that stars near the turnoff color dominated the plot out to our adopted outer limit. For M3 we adopted an annulus  $120 < r < 360$  arcseconds, while for M92 we adopted  $120 < r < 600$  arcseconds. For Carina we adopted the entire disk  $r < 600$  arcsec because we detected no inward increase in photometric scatter at any radius; apparently, crowding is not a limiting factor in our data for stars of any brightness within the magnitude range of interest at any radius all the way in to the center of the galaxy.

## 3. STELLAR EVOLUTIONARY MODELS

Most of the isochrones considered here were derived from the grids of evolutionary tracks that have been made publicly available by V14a, using their interpolation software, and converted to the observed planes via the transformations produced by CV14. Both the stellar models and the color- $T_{\text{eff}}$  relations can be interpolated to arbitrary  $\alpha$ -element abundances within the range  $-0.4 \leq [\alpha/\text{Fe}] \leq +0.4$  at nearly all of the  $[\text{Fe}/\text{H}]$  values of interest. (For this study, we have assumed  $Y = 0.25$  for the initial mass-fraction abundance of helium, though it is possible to generate isochrones from the V14a grids for any value of  $Y$  between 0.25 and 0.33.)

We have also made use of a few supplementary grids for  $[\text{Fe}/\text{H}] < -2.4$  that will be the subject of a forthcoming pa-

per on extremely metal-deficient stars (those having values of  $[\text{Fe}/\text{H}]$  as low as  $-4.0$ ). Some of these computations, which allow for variations in  $[\text{O}/\text{Fe}]$  from  $+0.4$  to  $+1.2$  at fixed  $[\text{Fe}/\text{H}]$  values, assuming  $[m/\text{Fe}] = +0.4$  for the other  $\alpha$ -elements, have been employed by Brown et al. (2014) to interpret their *Hubble Space Telescope* (*HST*) photometry of several UFD galaxies. In addition, we are in the process of generating fully consistent zero-age horizontal branches (ZAHBs) for all of the aforementioned grids and several of them appear in the plots that are presented in Section 4.1. (One of the V14a grids and three ZAHBs have been extended to sufficiently high masses to permit comparisons of stellar models with the observations of the intermediate-age TO stars in Carina and with the location of its red HB clump.)

### 3.1. Calibration of the Isochrones

As discussed at some length by V13 (also see V14a), there are so many uncertain factors that play a role in intercomparisons of predicted and observed CMDs (such as the distance and  $[\text{Fe}/\text{H}]$  scales, heavy-element mixtures, color transformations, convection theory, atmospheric boundary conditions, the role of diffusive and extra mixing processes) that “perfect” agreement between observations and theory is not a realistic expectation. It is, in fact, remarkable that current isochrones fare as well as they do, as the discrepancies that are found in, for instance, fits of current Victoria-Regina stellar models to GC photometry (see V14a, their Fig. 14) generally involve no more than relatively small zero-point and systematic offsets when well-supported estimates of the cluster properties are assumed. These offsets are typically at the level of  $\lesssim 0.025$  mag in the case of  $V - I_C$  colors (see CV14) and the very similar colors which can be derived from the *HST*  $F606W$  and  $F814W$  bandpasses (V13, V14a).

For the most part, isochrones seem to perform nearly as well on the  $(B - V, V)$ -diagram as on the  $(V - I_C, V)$ -plane (see the examples given by CV14). However, as discovered in the course of this study,  $B - V$  colors appear to become increasingly problematic at the lowest  $[\text{Fe}/\text{H}]$  values. Whereas the isochrones provide rather good fits to our  $BV$  data for M3 (comparable to those presented for M5 by CV14) when reasonable assumptions are made concerning its basic properties (i.e., distance, reddening, and metallicity), the agreement is noticeably less satisfactory in the case of M92. While the discrepancies are relatively minor above the turnoff, the models (for  $[\text{Fe}/\text{H}] = -2.40$ ; Kraft & Ivans 2008; Carretta et al. 2009a) predict an appreciably steeper MS slope than the observed one. It seems doubtful that this is due to problems with the model  $T_{\text{eff}}$  scale because the isochrones do not have similar difficulties when confronting M92 data derived from longer wavelength filters (e.g.,  $V - I_C$ , or the *HST* equivalent; see V13, V14a). It is even less likely that this difficulty can be attributed to observational errors because our CMD for M92 is based on a very large number of independently calibrated data sets (see § 2).

However, a resolution of this issue is not needed for this project. Since the  $BV$  observations of Carina, M3, and M92 have all been calibrated to the same photometric system, we can force the stellar models to be on very close to the same system if we simply correct the colors along the isochrones so that they reproduce the CMDs of the two GCs. Even though this does tie our analysis to particular distance and  $[\text{Fe}/\text{H}]$  scales for globular clusters, the resultant models should yield a more accurate interpretation of the Carina photometry than those without such adjustments. One must just be careful to

carry out this calibration of the synthetic colors in such a way that the latter vary smoothly with  $[\text{Fe}/\text{H}]$  (as well as with  $T_{\text{eff}}$  and  $\log g$ ) in order that they can be applied to isochrones for the ranges in age and metallicity found in Carina.

We believe that the best way to achieve this is to set up tables of  $\delta(B - V)$  values to complement the tabulated transformations to  $B - V$  given by CV14. As these results will be used primarily in the fitting of isochrones to the faintest TO of Carina, the color correction tables can be restricted to  $[\text{Fe}/\text{H}] = -3.0(0.5) - 1.5$ , and at each  $[\text{Fe}/\text{H}]$  value, to  $\log g = 2.5(0.5)5.0$  and  $T_{\text{eff}} = 5000(250)6750$  K, where the numbers in parentheses give the increments to the three variables. The color- $T_{\text{eff}}$  relations provided by CV14 consider exactly the same values of  $[\text{Fe}/\text{H}]$ ,  $\log g$ , and  $T_{\text{eff}}$  among their coverage of a greatly expanded parameter space (and  $\sim 40$  different color indices). They also provide tables for  $[\alpha/\text{Fe}] = -0.4(0.4) + 0.4$ , but the majority of the Galactic GCs appear to have  $[\alpha/\text{Fe}] \approx +0.4$  (see, e.g., Carretta et al. 2009b); consequently, the  $\delta(B - V)$  adjustments that are derived from a consideration of the M3 and M92 CMDs implicitly assume this value of  $[\alpha/\text{Fe}]$ . (In fact, we have not attempted to determine how  $\delta(B - V)$  depends on the abundances of the  $\alpha$ -elements. As shown below, these corrections are, in any case, quite small for the post-turnoff portions of Victoria-Regina isochrones, and since they are used in conjunction with the CV14 transformations, which do predict the effects on  $B - V$  of differences in  $[\alpha/\text{Fe}]$ , this neglect should not be a concern. In other words, we have assumed that, at a fixed value of  $[\text{Fe}/\text{H}]$ , the dependence of  $\delta(B - V)$  on  $\log g$  and  $T_{\text{eff}}$  is not a function of  $[\alpha/\text{Fe}]$ .)

M3 and M92 are particularly suitable GCs for this exercise because their  $[\text{Fe}/\text{H}]$  values are close to the grid values of  $-1.5$  and  $-2.5$ , respectively. Hence, whatever adjustments in the  $B - V$  color are needed to obtain good fits of isochrones to the CMDs of these systems will be very similar to the values that should appear in the interpolation tables for these metallicities. Because  $B - V$  is much more dependent on  $T_{\text{eff}}$  than on  $\log g$  (especially for MS, SGB, and lower RGB stars; see, e.g., VandenBerg & Clem 2003, their Fig. 3), the temperature shift, at a fixed gravity, between the MS portions of isochrones for  $[\text{Fe}/\text{H}] = -2.0$  and  $-2.5$ , as a fraction of that predicted for  $[\text{Fe}/\text{H}] = -1.5$  and  $-2.5$  isochrones of the same age, should be a reasonable approximation to the corresponding variation in  $\delta(B - V)$ . Based on our stellar models, this fraction is close to 0.30, which we have adopted in the creation of a table of color corrections for  $[\text{Fe}/\text{H}] = -2.0$  (and for  $-3.0$ , using a similar rationale). Indeed, with relatively few iterations, it was quite easy to produce a table of  $\delta(B - V)$  values that are smooth functions of  $[\text{Fe}/\text{H}]$ ,  $\log g$ , and  $T_{\text{eff}}$  and which enable isochrones to satisfy the M3 and M92 constraints very well. Importantly, these corrections are small for the age-sensitive parts of isochrones — easily within the uncertainties associated with the stellar models, color- $T_{\text{eff}}$  relations, and photometric zero-points.

This can be seen in Figure 2, which compares the transformations to  $B - V$  for  $[\text{Fe}/\text{H}] = -2.0$  (and  $[\alpha/\text{Fe}] = +0.4$ ) from CV14 (filled circles) with those obtained if the latter are corrected by our adopted values of  $\delta(B - V)$  (open circles). A 12 Gyr isochrone for the same chemical abundances has also been plotted to permit visual estimates of the variations in the color adjustments that have been applied as a function of evolutionary state. Above the turnoff, they amount to  $< 0.02$  mag, rising to  $\sim 0.04$  mag only at  $\log g \gtrsim 4.7$ . Lines of constant  $T_{\text{eff}}$  run in a nearly vertical direction; e.g., the bluest

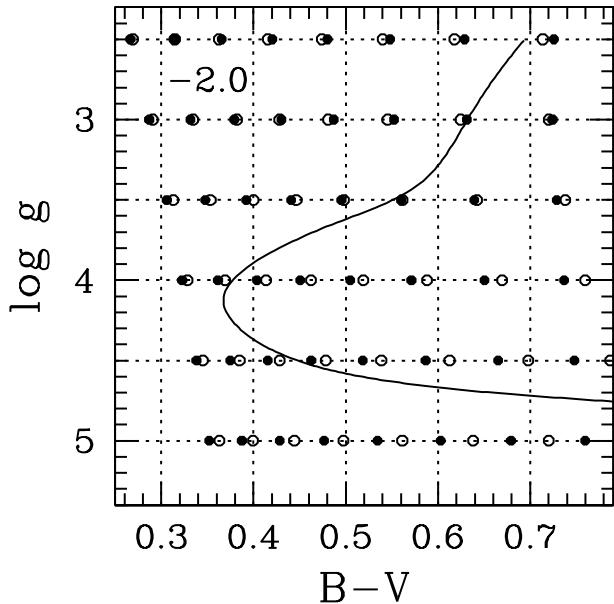


**Figure 2.** Plot of the  $(B-V)-T_{\text{eff}}-\log g$  relations for  $[\text{Fe}/\text{H}] = -2.0$ ,  $\log g = 2.5(0.5)5.0$  and, at constant gravity,  $T_{\text{eff}} = 6750(-250)5000$  K, in the direction from left to right. The filled and open circles give, in turn, the transformations reported by CV14 and those derived here from fits to isochrones to the M3 and M92 CMDs, and other considerations (see the text). The  $\delta(B-V)$  values referred to in the text correspond to the differences between the open and filled circles at common values of  $\log g$  and  $T_{\text{eff}}$ . The solid curve represents a 12 Gyr isochrone for  $[\text{Fe}/\text{H}] = -2.0$ ,  $[\alpha/\text{Fe}] = +0.4$ , and  $Y = 0.25$  (from V14a).

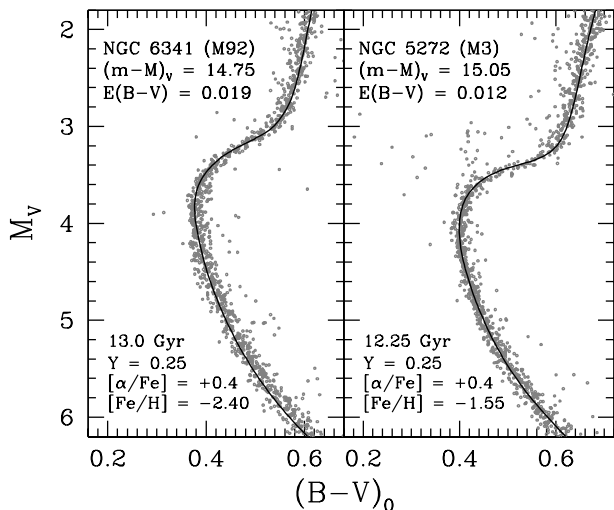


**Figure 3.** Fits of isochrones for the indicated ages and chemical abundances to our CMDs for M92 and M3 on the assumption of the apparent distance moduli (based on ZAHB models) and reddenings (from Schlafly & Finkbeiner 2011) that are specified in the upper left-hand corners of the respective panels. The predicted  $B-V$  colors were derived from the CV14 transformations, but with small adjustments to the latter that were obtained by interpolation in tables of  $\delta(B-V)$  values for  $[\text{Fe}/\text{H}] = -3.0, -2.5, -2.0$ , and  $-1.5$  and ranges of  $\log g$  and  $T_{\text{eff}}$  relevant to the faintest TO stars in Carina. (The differences between the adopted and CV14 color- $T_{\text{eff}}$  relations for stars having  $[\text{Fe}/\text{H}] = -2.0$  are illustrated in the previous figure.)

points at the grid values of  $\log g$  from 2.5 to 5.0 give the predicted colors at  $T_{\text{eff}} = 6750$  K, whereas the reddest ones indicate the colors for the coolest  $T_{\text{eff}}$  considered (5000 K). At a fixed gravity, the points at intermediate  $B-V$  values illustrate how this color index varies when the temperature decreases in successive steps of 250 K, in the direction from left to right.

Figure 3 demonstrates that our calibration of the CV14

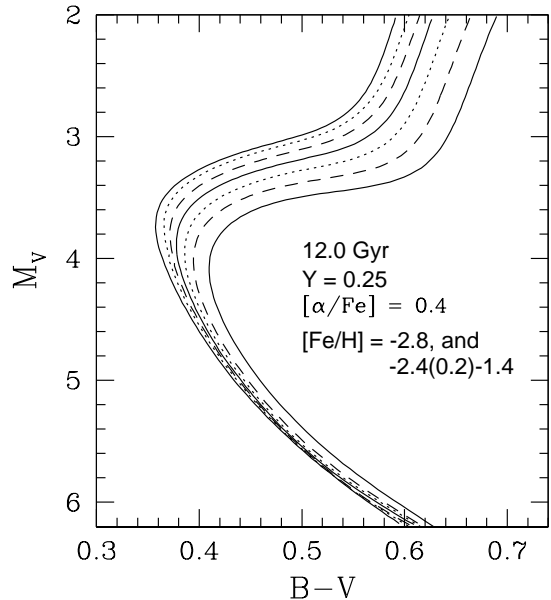


**Figure 4.** Plot of isochrones for the indicated age and chemical abundances if the modified CV14 transformations described in this paper are used to transpose them to the  $(B-V, M_V)$ -diagram.

transformations does, indeed, lead to excellent fits of isochrones to the CMDs of M3 and M92 (by design, of course), when the reddenings given by Schlafly & Finkbeiner (2011) and apparent distance moduli based on ZAHB models for the indicated chemical abundances are assumed. (Distances derived in this way are in very good agreement with those based on the RR Lyrae standard candle; see V13 and VandenBerg et al. 2014b, hereafter V14b.) It is worth pointing out that the same ages would be (and are) found using the CV14 color- $T_{\text{eff}}$  relations because the predicted TO luminosities have not been altered by the adopted  $\delta(B-V)$  offsets. The main effect of the latter, besides removing small discrepancies along the lower RGB, is to force the predicted and observed TO colors (and lower main sequences) to agree. This concurrence is required, in fact, if one is to obtain the best estimate of the turnoff age of a GC from fits of isochrones to just the small region of its CMD in the vicinity of the TO (see the discussion of this issue by V13, their § 3.1).<sup>5</sup> In any case, the colors along Victoria-Regina isochrones *should* be adjusted in the way that we have described if the ZAHB-based distance scale is accurate and the actual cluster  $[\text{Fe}/\text{H}]$  values are close to the values that we have adopted (see Fig. 3).

To further illustrate the performance of the calibrated transformations to  $B-V$ , we have plotted, in Figure 4, isochrones for seven  $[\text{Fe}/\text{H}]$  values (as indicated), each assuming  $Y = 0.25$ ,  $[\alpha/\text{Fe}] = +0.4$ , and an age of 12 Gyr. The differences between them, at a fixed value of  $M_V$ , vary smoothly and monotonically, and there are no obvious irregularities as a function of absolute magnitude or color. The main effect of the  $\delta(B-V)$

<sup>5</sup> The main reason why V13 obtained ages for M3 and M92 that are 0.5 Gyr younger than those derived here — despite their assumption of slightly smaller distance moduli by 0.03 mag, which would normally imply *increased* ages by  $\approx 0.3$  Gyr — is that the model grids used in their study assumed higher oxygen abundances by 0.24 dex (in an absolute sense), due to differences in the respective solar heavy-element mixtures and the adopted values of  $[\text{O}/\text{Fe}]$ . The higher the absolute oxygen abundance, the lower the age at a given TO luminosity (see V12). This example serves to illustrate the importance of taking chemical composition and distance modulus differences into account when comparing age determinations for the same star cluster that are reported in different papers.

values that we have generated is to displace the lower-MS portions of the isochrones to redder colors, especially at  $[\text{Fe}/\text{H}] \lesssim -1.8$ , by amounts that vary directly with  $M_V$ . As a result, the isochrones display a considerably reduced sensitivity to  $[\text{Fe}/\text{H}]$  over the range  $4 \lesssim M_V \lesssim 6$ , as required by the photometry of M3 and M92 (if our assumed properties for them are accurate), compared with their behavior when the CV14 transformations are used without any adjustments.

Figs. 2, 3, and 4 thus give us considerable confidence that the isochrones used in this investigation to model the oldest MS, SGB, and lower RGB stars in Carina are about as well constrained to empirical data as we are able to make them. In the case of giant stars (those with  $\log g \lesssim 2.5$ ), the CV14 transformations to  $B-V$  appear to require no more than a  $-0.01$  mag adjustment in order for the same isochrones that have been plotted in Fig. 3 to reproduce the entire RGBs of M3 and M92 (see § 4.3, which presents an analysis of the giant-branch populations of the dSph). Finally, we note that the interpolated  $\delta(B-V)$  values for  $T_{\text{eff}} = 6750$  K are used when the predicted temperatures exceed this limit (as in isochrones that are relevant to IA stars), and the tabulated color adjustments for  $[\text{Fe}/\text{H}] = -1.50$  are adopted for slightly more metal-rich stars. The latter is a reasonable assumption given that the CV14 transformations appear to provide comparable fits of isochrones to the CMD of M5 (see CV14), which has  $[\text{Fe}/\text{H}] \sim -1.3$  (e.g., Carretta et al. 2009a), and of the  $\sim 0.2$  dex more metal-deficient cluster M3, as we found during the course of this work. Moreover, there appear to be very few stars in the faintest TO of Carina with  $[\text{Fe}/\text{H}] > -1.5$  (see Fig. 1a); consequently, they will have no more than a very minor influence on our findings.

#### 4. INTERPRETATION OF THE CARINA CMD

To try to constrain our understanding of Carina, we will first intercompare its CMD with that of M92. In addition to highlighting some of the similarities and differences between these systems, this will provide a useful check of the reliability of the adopted reddenings and distance moduli in a relative sense. This will be followed by fits of isochrones that utilize the empirically calibrated color transformations just described to the CMD of the galaxy, to explore the implications of different assumptions concerning the ages and chemical compositions of its stellar populations. Fully consistent ZAHB loci will also be considered. Whereas the analyses presented in the first subsection will reveal some of the possible interpretations of Carina’s CMD, with particular emphasis on the oldest stars, the next one will endeavor to assess the viability of these possibilities through numerical simulations. What does the observed MDF and the luminosity width of the SGB associated with the faintest TO tell us about the SFH? The third, and final, subsection will examine the thin RGB of Carina to ascertain the extent to which it is the outcome of a fortuitous alignment of the ages and metallicities of the stars that populate this feature.

##### 4.1. Turnoff and HB Stars in Carina

In the upper panel of Figure 5, the CMD of M92 has been transposed to the  $[(B-V)_0, M_V]$ -diagram assuming (as adopted previously; see Fig. 3)  $E(B-V) = 0.019$  and  $(m-M)_V = 14.75$ . This apparent distance modulus is obtained if a ZAHB for  $Y = 0.25$  and  $[\text{Fe}/\text{H}] = -2.40$  (the solid curve) is fitted to the lower bound of the distribution of the cluster HB stars (as shown). To obtain this result, the synthetic

$B-V$  colors along the ZAHB were adjusted to the red by 0.016 mag, which is obtained from our  $\delta(B-V)$  tables if  $[\text{Fe}/\text{H}] = -2.40$  and  $T_{\text{eff}} \geq 6750$  K. Interestingly, V14b (see their Fig. 5) found that the same ZAHB provided an equally good fit to the HB of M92 on the  $[(V-I_C)_0, M_V]$ -diagram, but without having to apply any adjustment of the synthetic colors (from CV14). Essentially the same thing was found by V13 (see their Fig. 11) in a study of the nearly equivalent CMD of M92 that they constructed from the *HST*  $F606W, F814W$  observations that were obtained by Sarajedini et al. (2007) — though the stellar models employed in the 2013 investigation assumed a somewhat different metals mixture. [While the main cause of such minor inconsistencies is difficult to determine, it should not be a surprise that they exist given that, e.g., on-going improvements to model atmospheres and the line lists used in synthetic spectra are bound to affect the magnitudes derived from some filter bandpasses more than others. In particular,  $B$  is affected by line blanketing more than  $V$  and  $I_C$ ; consequently,  $B-V$  will be a more challenging color index to model than  $V-I_C$ .]

If the reddening in the direction of Carina is  $E(B-V) = 0.054$  (Schlafly & Finkbeiner 2011), the adoption of  $(m-M)_V = 20.28$  results in the superposition of the Carina and M92 CMDs shown in the top panel. In this case, the cluster SGB is coincident with the location of the densest concentration of Carina subgiants that are associated with the faintest TO, implying a similar age if the latter have the same metallicity. However, judging from the very different luminosity widths of their respective SGBs, the oldest stellar population in Carina must span a much wider range in age or metallicity, or both, than the stars residing in M92. (These indications from photometry have, of course, been confirmed by several spectroscopic studies; see § 1.) The assumed reddenings and distance moduli also imply that the RGB and HB of M92 lie along the blue edges of the galactic distribution of giants and horizontal branch stars, respectively, which is consistent with M92 being more metal-poor than the majority of the stars in Carina. Encouragingly, the adopted apparent modulus implies a true distance modulus of  $(m-M)_0 \approx 20.11$ , which is in very good agreement with recent determinations based on near-IR magnitudes of the RGB tip (20.08–20.12, Pietrzyński et al. 2009), on the RR Lyrae variables, (20.09, Coppola et al. 2013), and on the dwarf Cepheids in Carina (20.17, Vivas & Mateo 2013).

The location of the ZAHB for  $[\text{Fe}/\text{H}] = -2.4$  relative to the blue HB stars in Carina is more easily seen in the bottom panel, along with the same isochrone (for 13 Gyr) that matches the TO and SGB of M92. This isochrone lies below most, but not all, of the faintest subgiants in the dSph: a better match to the least luminous SGB stars is clearly provided by a 13 Gyr isochrone for  $[\text{Fe}/\text{H}] = -2.0$ . However, this is no more than suggestive, given that the assumed value of  $[\alpha/\text{Fe}]$  in these models is too high (recall Fig. 1a), and because a similar fit could be obtained using an even more metal-rich isochrone for a somewhat younger age. Still, these computations give the impression that Carina contains stars at least as old as those found in the most metal-poor GCs ( $\sim 13$  Gyr). In addition, they illustrate that the luminosity width of Carina’s SGB is consistent with a range in age  $\gtrsim 4$  Gyr, at a fixed  $[\text{Fe}/\text{H}]$  (note the separation between the 9 and 13 Gyr isochrones for  $[\text{Fe}/\text{H}] = -2.0$ ), or a variation in metallicity, at a given age, that is much larger than 0.4 dex (note that the 13 Gyr isochrones for  $[\text{Fe}/\text{H}] = -2.0$  and  $-2.4$  enclose only a

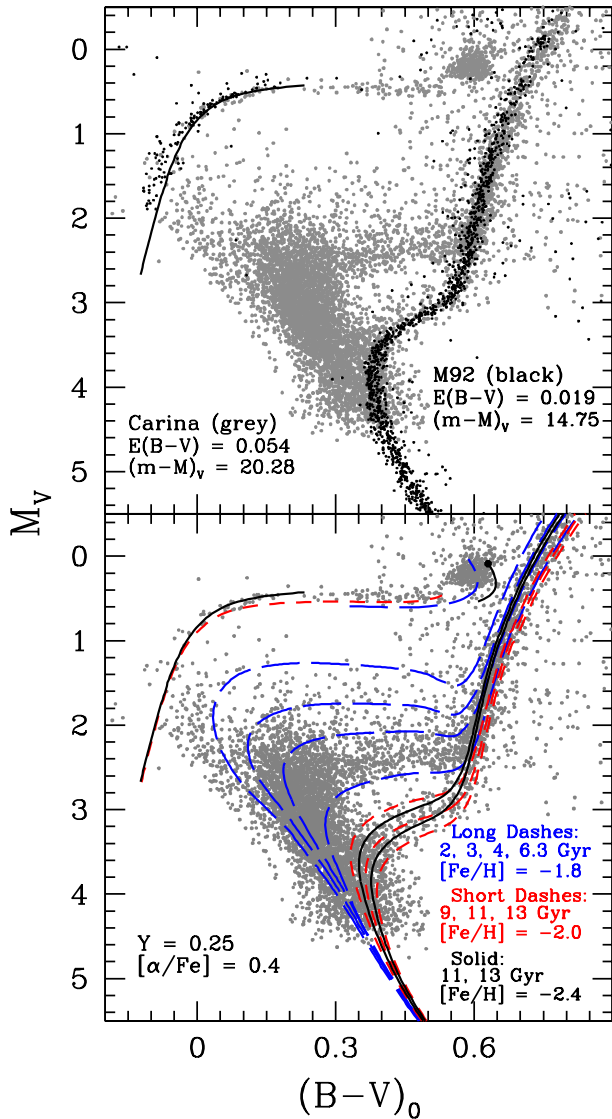


**Figure 5.** *Upper panel:* Superposition of the M92 CMD onto that of Carina assuming the indicated values of the reddening and apparent distance moduli. The solid curve represents a ZAHB for  $[\text{Fe}/\text{H}] = -2.40$ ,  $[\alpha/\text{Fe}] = +0.40$ , and  $Y = 0.25$ . *Lower panel:* Overlay of isochrones for the indicated chemical abundances and ages, along with fully consistent ZAHB loci, onto the CMD of Carina. Only the red end of the ZAHB is shown for  $[\text{Fe}/\text{H}] = -1.8$  and  $[\alpha/\text{Fe}] = +0.4$  (long dashes), as well as the one for  $[\text{Fe}/\text{H}] = -1.4$  and  $[\alpha/\text{Fe}] = 0.0$  (the curve with a small filled circle attached to the bright end).

small fraction of the observed subgiants).

The other isochrones which have been plotted indicate that little or no star formation occurred in a 2–3 Gyr period prior to the major SF burst that happened about 6 Gyr ago, and that there *may* have been a lull in the SF activity  $\sim 2.5$  Gyr ago as there is some (albeit marginal) indication of enhanced numbers of MS stars at both younger and somewhat older ages. It is worth mentioning that, if isochrones for  $Y = 0.25$ ,  $[\text{Fe}/\text{H}] = -1.4$ , and  $[\alpha/\text{Fe}] = +0.13$  (parameters that are also consistent with the  $[\alpha/\text{Fe}]$  vs.  $[\text{Fe}/\text{H}]$  relation shown in Fig. 1a) were compared with the Carina CMD, we would obtain an age of 5.9 Gyr for the oldest of the intermediate-age stars (as compared with 6.3 Gyr if they have  $[\text{Fe}/\text{H}] = -1.8$  and  $[\alpha/\text{Fe}] = +0.4$ ; see Fig. 5). The metallicity dependence of this age estimate is thus quite small — because the change in the absolute oxygen abundance between these two cases is only

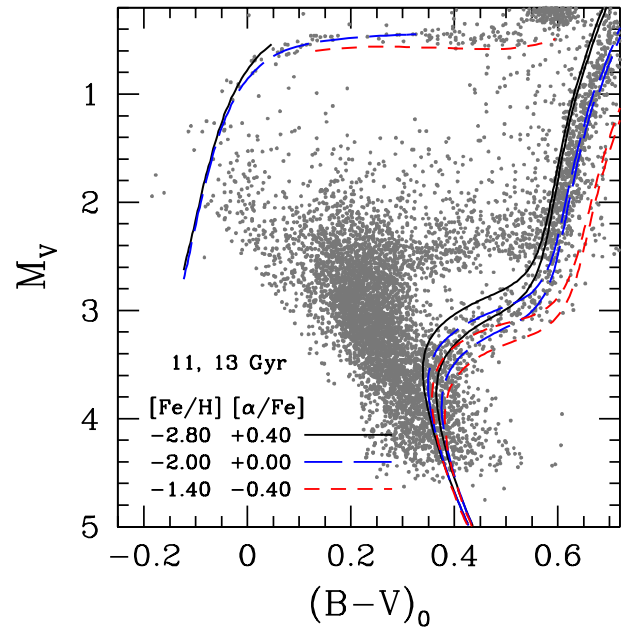


**Figure 6.** Similar to the bottom panel in the previous figure, except that isochrones and ZAHBs for values of  $[\text{Fe}/\text{H}]$  and  $[\alpha/\text{Fe}]$  that are more consistent with spectroscopic determinations (see Fig. 1a) are compared with the Carina CMD.

0.13 dex. As discussed by V12, isochrones for the same oxygen abundance (i.e.,  $[\text{O}/\text{H}]$ ), but different  $[\text{Fe}/\text{H}]$ , will predict nearly identical TO luminosity vs. age relations (especially at low metallicities, where the contributions of the metals to the opacities in the interiors of stars are small).

Aside from a 1–2 Gyr reduction in the absolute ages, these results are quite similar to those reported by, e.g., Hurley-Keller et al. (1998). The use of modern isochrones that take diffusive processes, recent advances in nuclear reaction rates, etc., into account can be expected to have some impact on age determinations, even if the same distances and chemical abundances are assumed. It is perhaps especially encouraging that current stellar models are able to reproduce the morphologies and the locations of the different photometric sequences in Carina very well once relatively small adjustments are made to the predicted  $B-V$  colors. Something worth mentioning is that, as shown many years ago by, e.g., Castellani & Degl’Innocenti (1995, and references therein), isochrones for young ages and very low metallicities have relatively smooth turnoffs, in stark contrast with the pronounced blueward hook features that are characteristic of their counterparts at near solar abundances. In a qualitative sense, our 2–4 Gyr isochrones look very similar to those computed  $\gtrsim 20$  years ago. (Because the model grids used in this study are limited to ages  $\gtrsim 5$  Gyr, the remainder of this paper will concentrate on just the oldest stellar populations of Carina.)

Figure 6 illustrates the superposition on the Carina CMD of 11 and 13 Gyr isochrones for metallicities that span nearly the full ranges in  $[\text{Fe}/\text{H}]$  and  $[\alpha/\text{Fe}]$  that have been derived spectroscopically. (Fully consistent ZAHBs, to be discussed near the end of this subsection, are also shown.) In confirmation of the remarks made above concerning the oxygen abundance, the isochrones for  $[\text{Fe}/\text{H}] = -2.0$  and  $[\alpha/\text{Fe}] = 0.0$  predict very similar turnoff and SGB luminosities as those for the same ages but for  $[\text{Fe}/\text{H}] = -2.40$  and  $[\alpha/\text{Fe}] = +0.4$  (see the previous figure). Both assume exactly the same value of  $[\text{O}/\text{H}]$  and, as a close inspection of both plots reveals, their

locations relative to the observed TO and SGB stars in their vicinity are nearly the same. However, the RGB portions of these isochrones are obviously not coincident, but that can be attributed to the differences in the abundances of the heavier metals, notably the iron-peak elements. Varying the oxygen abundance does not affect the location of the RGB at low metallicities (see V12).

Similarly, considering the isochrones for  $[\text{Fe}/\text{H}] = -2.8$  and  $[\alpha/\text{Fe}] = +0.4$ , on the one hand, and those for  $[\text{Fe}/\text{H}] = -2.0$  and  $[\alpha/\text{Fe}] = 0.0$ , on the other, it is readily understood that it is the 0.4 dex difference in  $[\text{O}/\text{H}]$  which is primarily responsible for the  $\sim 1$  Gyr difference in age at a given TO luminosity (see Fig. 6). Although the abundances of the iron-peak elements differ by 0.8 dex, and those of the other  $\alpha$ -elements (Ne, Mg, Si, ...) differ by 0.4 dex, these variations mainly cause a small shift in the model  $T_{\text{eff}}$  scale due to their effects on the atmospheric opacities (see V12). The implication of these results is that the age at a given TO luminosity varies quite weakly with position along the sloped parts of the  $[\alpha/\text{Fe}]$  vs.  $[\text{Fe}/\text{H}]$  relation shown in Fig. 1a. Conversely, a given subgiant thickness would imply a narrower range in  $[\text{Fe}/\text{H}]$ , at a common age, if  $[\alpha/\text{Fe}] = \text{constant}$  than if  $[\alpha/\text{Fe}]$  and  $[\text{Fe}/\text{H}]$  are anti-correlated (as observed).

This undoubtedly helps to explain why Bono et al. (2010) argued that the oldest TO/SGB stars in Carina span a significantly smaller range in  $[\text{Fe}/\text{H}]$  than that derived from spectroscopic work. They reached this conclusion as the result of (i) comparing the fiducial sequences for a few of the Galactic GCs, which have  $[\alpha/\text{Fe}] \approx 0.4$ , with the Carina CMD, and (ii) examining synthetic CMDs that were derived from isochrones for  $[\alpha/\text{Fe}] = 0.0$  and a wide range in  $[\text{Fe}/\text{H}]$ . Both of these avenues assumed, either directly or indirectly, constant  $[\alpha/\text{Fe}]$ ; in which case, isochrones of similar age but different  $[\text{Fe}/\text{H}]$  (and  $[\text{O}/\text{Fe}]$ , since  $\delta[\text{O}/\text{H}] = \delta[\text{Fe}/\text{H}]$ ) will predict a larger difference in their TO/SGB luminosities than one expects if  $[\alpha/\text{Fe}]$  decreases with increasing  $[\text{Fe}/\text{H}]$ . What is of critical importance in this discussion is how  $[\text{O}/\text{H}]$  (which is equivalent to the absolute O abundance, if the models being compared assume the same solar abundances) varies with  $[\text{Fe}/\text{H}]$ .

Perhaps the most compelling argument presented by Bono et al. (2010) is that, as demonstrated in their CMD simulations, the component of Carina's HB that is populated by its oldest stars is too thin to be consistent with the range in  $[\text{Fe}/\text{H}]$  that has been derived in spectroscopic studies. Indeed, this is also suggested by the ZAHB models that appear in the bottom panel of Fig. 5. Most of the old core He-burning stars (i.e., those populating the nearly flat portion of the HB at  $(B-V)_0 \lesssim 0.55$ ), are brighter than the ZAHB for  $[\text{Fe}/\text{H}] = -2.0$  (the short-dashed curve) and fainter than the one for  $[\text{Fe}/\text{H}] = -2.4$  (the solid curve). Moreover, there is no evidence at all for old HB stars with  $[\text{Fe}/\text{H}] \gtrsim -1.8$  as they should lie below the ZAHB represented by the long-dashed curve.

Before moving to the next figure, note that the last of these three ZAHBs, which has been extended to a mass that is predicted for a 2 Gyr RGB tip star, reaches close to the maximum luminosity of the HB clump (as shown). Encouragingly, a star of the same  $[\text{Fe}/\text{H}]$  that has an RGB tip age of 6 Gyr (approximately the age of the oldest IA stars) is predicted to reach its ZAHB location at close to the minimum luminosity of the clump (at the location of the long-dashed curve). According to our models, and consistent with the observed MDF to within its uncertainties, few of the observed HB clump stars are predicted to have  $[\text{Fe}/\text{H}] > -1.4$  (which has been assumed, together with  $[\alpha/\text{Fe}] = 0.0$ , in the computation of the ZAHB to

which a small filled circle has been attached at its bright end), since this ZAHB matches the red edge of the distribution of HB clump stars. (These abundances are consistent with the variation of  $[\alpha/\text{Fe}]$  with  $[\text{Fe}/\text{H}]$  given by the solid curve in Fig. 1a.) To reinforce this point, a ZAHB for  $[\text{Fe}/\text{H}] = -1.2$  and  $[\alpha/\text{Fe}] = 0.0$  would have been located well to the red of the HB clump, almost intersecting the observed RGB, had we chosen to plot this case. (There may well be some stars in our CMD that have  $[\text{Fe}/\text{H}] \sim -1.2$ , in accordance with spectroscopic findings, but the small minority of such stars presumably does little more than contribute to the scatter in the vicinity of the HB.)

The benefits of being able to compare observations with stellar models *for the observed chemical abundances* is further revealed by the ZAHBs that have been plotted in Fig. 6. They show that the small luminosity width of Carina's old HB does not preclude the presence of stars with  $[\text{Fe}/\text{H}]$  values that vary by more than 1 dex, *provided* that  $[\alpha/\text{Fe}]$  varies with  $[\text{Fe}/\text{H}]$  in approximately the observed way (i.e., following the trend given by the dashed line in Fig. 1a). The ZAHB for  $[\text{Fe}/\text{H}] = -1.4$  and  $[\alpha/\text{Fe}] = -0.4$  provides quite a good fit to the faintest of the cluster HB stars that are fainter than the clump stars and that have  $0.35 \lesssim (B-V)_0 \lesssim 0.55$ . This is not unexpected since, as reported by VandenBerg et al. (2000), the luminosity of a ZAHB is quite a strong, inverse function of  $[\alpha/\text{Fe}]$ , at fixed values of  $[\text{Fe}/\text{H}]$  and  $Y$ .<sup>6</sup>

To be sure, the distribution of the stars relative to the three ZAHBs that have been plotted in Fig. 6 seems anomalous. Most of the observed HB stars are fainter and redder than the ZAHB for  $[\text{Fe}/\text{H}] = -2.0$  and  $[\alpha/\text{Fe}] = 0.0$ , implying that they are more metal rich, which is obviously in conflict with the MDF. A possible solution to this dilemma is that the oxygen abundance is significantly higher than  $[\text{O}/\text{Fe}] = +0.4$  in (at least) the most metal-deficient stars in Carina, and that it remains offset from the  $[m/\text{Fe}]$  values of the other  $\alpha$ -elements by  $\sim 0.2$  dex (or more?) as  $[\alpha/\text{Fe}]$  decreases with increasing  $[\text{Fe}/\text{H}]$ . For instance,  $[\text{O}/\text{Fe}] \gtrsim +0.6$  is generally found in Milky Way halo stars (e.g., Fabbian et al. 2009, Ramírez et al. 2012, V14b), whereas a smaller enhancement ( $[m/\text{Fe}] = 0.3-0.4$ ) is generally found for Mg, Si, Ca, Ti, etc. (see, e.g., Cayrel et al. 2004). At low metallicities, a ZAHB is stretched to redder colors and fainter luminosities over a considerable fraction of its length as the absolute oxygen abundance is increased (see, e.g., VandenBerg & Bell 2001; their Fig. 6). (At higher  $[\text{Fe}/\text{H}]$ , enhanced  $[\text{O}/\text{H}]$  mainly causes a redward displacement of just the red end of a ZAHB.) Thus, higher oxygen could shift the ZAHB loci for  $[\text{Fe}/\text{H}] \lesssim -2.0$  in just the way that is needed to reconcile them with the locations of a significant fraction of the reddest stars in the "old" HB component of Carina. Unfortunately, little seems to be known about the  $[\text{O}/\text{H}]$  values in Carina stars, and it must be left for future

<sup>6</sup> Work is in progress by D.A.V. to produce ZAHB loci for all of the chemical abundance choices considered by V14a, and we leave a detailed discussion of those ZAHBs to the forthcoming paper. However, it may be of some interest to note that, despite the revisions which have been made to the Victoria evolutionary code over the past 15 years, current ZAHB models predict very similar luminosities for RR Lyrae stars as those presented by VandenBerg et al. (2000). Whereas the latter neglected diffusion physics and assumed a primordial helium abundance corresponding to  $Y = 0.235$ , which was the favored value at that time, current Victoria models take the gravitational settling of helium into account while assuming the current best estimate of the primordial value of  $Y$  ( $\approx 0.250$ ; e.g., Komatsu et al. 2011). Fortunately, this increase in  $Y$  largely compensates for the effects of diffusion on the properties of RGB tip stars (primarily the envelope helium abundance) that control the predicted luminosity of the HB.



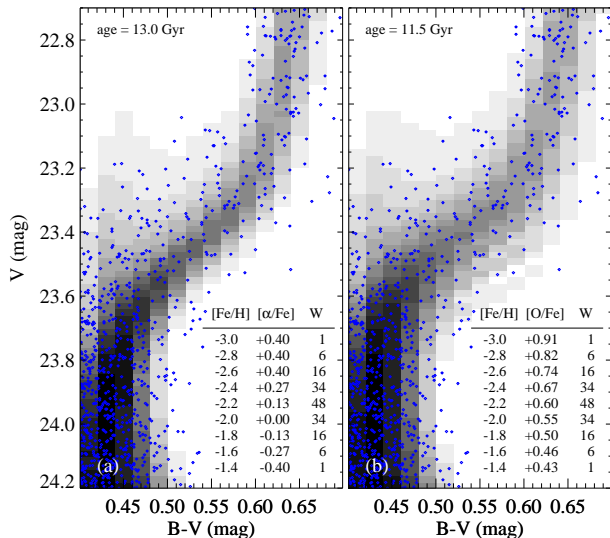


**Figure 7.** Best-fit model (grey shading) for the oldest Carina stars (blue points), assuming a single burst of star formation and the [Fe/H] distribution of Figure 1b. The relative weights ( $W$ ) are also specified in the inset table for each panel. The  $\alpha$ -varying model produces a much narrower SGB than observed (left panel). The O-varying model (with [ $\alpha$ /Fe] otherwise held at +0.4) produces a somewhat broader SGB that is still narrower than observed (right panel).

work, both observational and theoretical, to investigate these speculations.

Figure 6 also suggests that the faintest SGB stars are old, iron-rich,  $\alpha$ -poor stars. (The delay time between SF and the onset of SN Type Ia explosions is not necessarily an argument against the near coevality of stars with very different [ $\alpha$ /Fe] values, as it can be as short as  $\sim 100$ – $500$  Myr or as long as a few Gyr, depending on, among other things, whether the star formation rate is high or low, respectively; see the review by Maoz et al. 2014.) It is possible that some of them are field stars, though we have tried to remove such objects. Alternatively, it may be that the actual [O/Fe] values are higher than those implied by the assumed values of [ $\alpha$ /Fe]. This would have the effect of reducing the predicted age at a given TO luminosity, or equivalently, of shifting isochrones for a fixed age and [Fe/H] to higher  $M_V$ . That is, the faintest SGB stars could be very old stars with low iron, and relatively high oxygen, abundances (that evolve to red ZAHB locations). To provide a limited investigation of the consequences of this possibility for the oldest TO/SGB stars in Carina, some of the simulations presented in the next subsection will make use of the model grids for [ $\alpha$ /Fe] = +0.4 and high values of [O/Fe] that were employed in the recent study of several UFD galaxies by Brown et al. (2014).

#### 4.2. Simulations of the SFH of the Oldest Stellar Populations

To explore the SFHs that are consistent with the oldest populations in Carina under different metallicity assumptions, we have constructed several synthetic CMDs in the  $B$  and  $V$  bands, employing the same calibrated isochrone library described above. Two different SFH scenarios have been explored: a short burst of star formation with an idealized MDF (Fig. 1b), and an extended period of star formation lasting several Gyr, with only loose constraints on the MDF. In each of these two SFH scenarios, the relationships for [ $\alpha$ /Fe] vs. [Fe/H] and [O/Fe] vs. [Fe/H] were also varied. A linear combination of synthetic CMDs, each representing a partic-

ular age and metallicity, was used to fit the observed CMD. These fits were performed via the minimization of the Poisson maximum likelihood statistic of Dolphin (2002), and the quality of the best fit was evaluated by comparing the best-fit score to the distribution of such scores arising from Monte Carlo realizations of the photometric data.

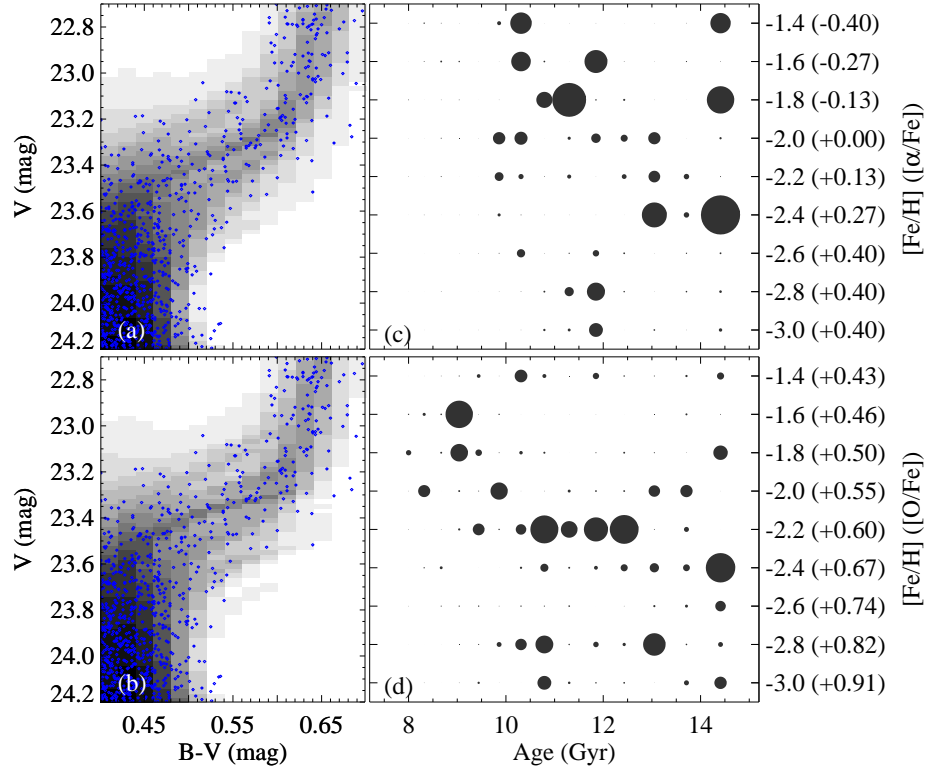
Usually, synthetic CMDs are constructed using the results of artificial star tests. Such tests characterize the photometric uncertainties and incompleteness as a function of position within the CMD, allowing each point along an isochrone to be scattered in the synthetic color-magnitude plane. Due to the heterogeneous nature of the observations studied here, artificial star tests are impractical, but the photometry of each star in the catalog comes from many individual exposures, such that the photometric uncertainties are well understood. Furthermore, for the CMD region being simulated, the photometric errors are small ( $< 0.05$  mag); consequently, the completeness should be near 100%. For these reasons, we used the photometric errors from the catalog to define a Gaussian scattering kernel as a function of position within the CMD.

The synthetic CMDs were populated using a Salpeter (1955) initial mass function (IMF), although the small mass range of stars in the fitting region ( $< 0.1 M_{\odot}$ ) makes the assumed IMF unimportant. We assumed a binary fraction of 14% (Minor 2013), but the results would not change significantly if we were to adopt a value closer to 50%, which is typically found in other dwarf galaxies. To fit the SFH of the oldest population, we isolated the faintest SGB stars in the catalog, along with its neighboring stars in the vicinity of the MSTO and the lower RGB (see Figure 7).

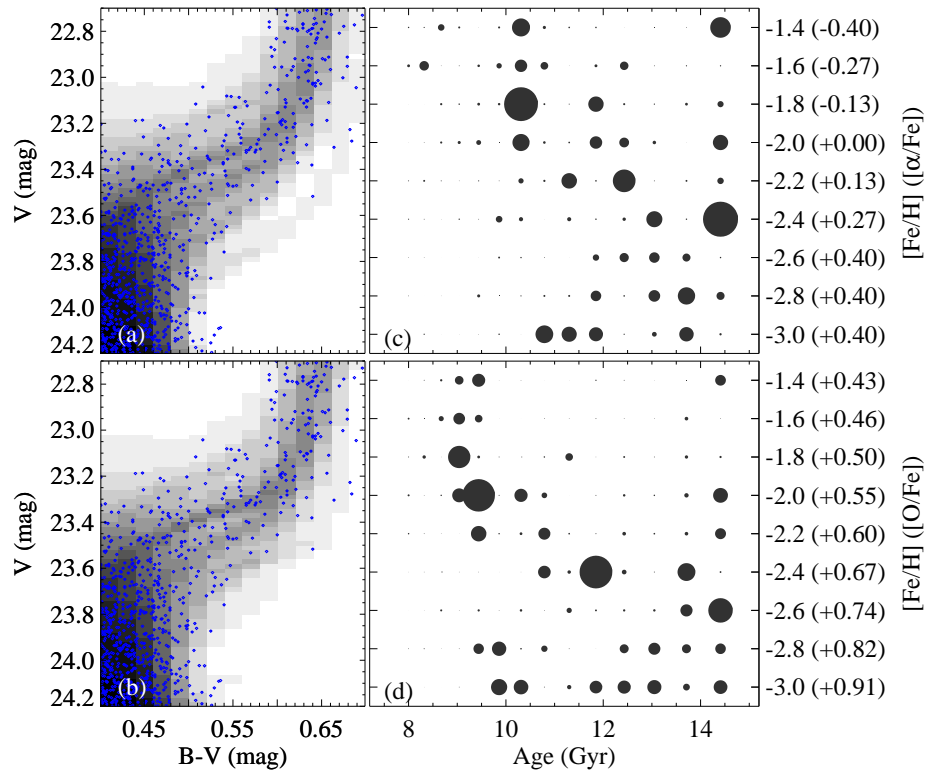
We begin with a simple model in which (i) the star formation is assumed to occur in a single burst, and (ii) the variation in the number of stars as a function of [Fe/H] corresponds to the MDF shown in Fig. 1b. However, we have explored two distinct assumptions regarding [ $\alpha$ /Fe] and [O/Fe]. The first is the “ $\alpha$ -varying” model, where [ $\alpha$ /Fe] increases with decreasing [Fe/H] (as in Figure 1a). The second is the “O-varying” model, where [O/Fe] increases with decreasing [Fe/H], while all other  $\alpha$  elements are held at a constant [ $\alpha$ /Fe] = +0.4 (as typically found in old, very metal-poor populations). The adopted relation between [O/Fe] and [Fe/H] is the same as that assumed by Brown et al. (2014), which is based on data presented by Frebel (2010).

Figure 7a shows the best-fit burst with the  $\alpha$ -varying model. The simulated SGB is significantly narrower than the observed SGB, resulting in a rather poor fit ( $\chi^2_{\text{eff}}=1.8$ ). Figure 7b shows the best-fit burst in the case of the O-varying model. The simulated SGB is broader, but still not as broad as that observed, again producing an unsatisfactory fit ( $\chi^2_{\text{eff}}=1.4$ ). Although not shown here, we note that a model in which all of the  $\alpha$ -elements, including oxygen, have a constant enhancement (specifically, [ $\alpha$ /Fe] = +0.4) for all [Fe/H] values looks quite similar to that illustrated in Figure 7b. Both of these fits are ruled out at more than  $6\sigma$ . Thus, if the MDF in the oldest population of Carina is similar to that shown in Figure 1b, it is unlikely to be a single-age population.

We now turn to a model with a more complex SFH, shown in Figure 8. Instead of a single burst, the age distribution is only restricted to the range of 8 to 14.4 Gyr. The MDF is constrained to iron abundances  $-3.0 \leq [\text{Fe}/\text{H}] \leq -1.4$ , as in the case of the single burst models, but it is permitted to take any form within this range. (These fits were performed using the StarFISH code of Harris & Zaritsky 2001.) Our results



**Figure 8.** Best-fit model (grey shading) for the oldest Carina population (blue points), assuming an extended SFH. Metallicities are constrained to the  $[\text{Fe}/\text{H}]$  range in Figure 1b, with both an  $\alpha$ -varying model (*panel a*) and an O-varying model (*panel b*). Associated with each synthetic CMD, we show the best-fit SFH (*panels c and d*), with the area of each circle indicating the weight at that point in the grid of age and  $[\text{Fe}/\text{H}]$ .



**Figure 9.** As in Figure 8, but for an assumed distance modulus that is 0.1 mag larger.

for an  $\alpha$ -varying model and an O-varying model are shown in the upper and lower panels, respectively. For both cases,  $\chi_{\text{eff}}^2 = 1.2$  (rounded to one decimal place), but the O-varying fit is the slightly better one. However, although nearly the same value of the goodness-of-fit statistic is obtained, the derived weighting of the isochrones in Fig. 8d resembles the observed MDF more so than that shown in Fig. 8c. In particular, the former simulation predicts more stars with  $[\text{Fe}/\text{H}] \sim -2.2$  (recall Fig. 1b) than in lower or higher metallicity bins, whereas the opposite is found in the latter simulation.

It may be recalled that the results presented in Fig. 8c were anticipated by the overlays of isochrones to the Carina CMD discussed previously. As shown in Fig. 6, isochrones for high ages and  $[\text{Fe}/\text{H}]$  values are apparently needed to explain the faintest SGB stars if the assumed  $\alpha$ -element abundances follow the adopted relation between  $[\alpha/\text{Fe}]$  and  $[\text{Fe}/\text{H}]$ . As indicated by the simulation results in Fig. 8d, this is not the case if the stellar models allow for high oxygen abundances. Also worth mentioning is the fact that significantly higher ages, at a fixed metallicity, would have been found had we neglected diffusive processes (see, e.g., VandenBerg et al. 2002, their Fig. 2). (However, if such physics is ignored, it would become especially difficult to reconcile stellar ages with the age of the universe; see V14b.)

Although the fits are not perfect, both of the cases considered in Fig. 8 demonstrate that the oldest population in Carina can be reproduced if the star formation epoch lasted a few Gyr. Although there is a general trend of decreasing age at increasing metallicity, the particular distribution of the points in the age-metallicity plane depends quite sensitively on how  $[\text{O}/\text{Fe}]$  varies with  $[\text{Fe}/\text{H}]$ , and the distance modulus assumed. A shorter distance would be more problematic than a longer distance because it would imply that all of the stars (notably those on the SGB) have fainter  $M_V$  values, thereby making them older. As a consequence, the weighting of the isochrones found for the O-varying model (Fig. 8d) would move in the direction of that obtained for the  $\alpha$ -varying model (Fig. 8c), and the results for the latter case would be skewed to even older ages and higher  $[\text{Fe}/\text{H}]$  values (in greater conflict with the observed MDF).

Figure 9 shows that the opposite trend is found if a slightly larger distance modulus (by 0.1 mag) is assumed. Comparing, e.g., Fig. 9c with Fig. 8c reveals that the distribution and weighting of the points has been shifted to lower  $[\text{Fe}/\text{H}]$  values. That is, the models predict larger fractions of older, more metal-poor stars if the distance to Carina is 0.1 mag larger than our adopted (ZAHB-based) modulus. (The same thing, which may seem counter-intuitive, is implied by the differences between Figs. 9d and 8d.) As a consequence, the  $\alpha$ -varying model provides a more agreeable fit to the observations, while the O-varying model seems to be somewhat less satisfactory. However, the main value of the simulations presented in Figs. 8 and 9 is to illustrate how they are affected by parameter variations. To obtain accurate and robust age determinations, it is clearly of paramount importance to have reliable abundances of the individual  $\alpha$ -elements (especially O, but also Mg and Si; see V12) so that their variations with  $[\text{Fe}/\text{H}]$ , as well as the observed star-to-star scatter of  $[m/\text{Fe}]$  at a fixed iron abundance, can be taken into account when simulating the observed CMD of Carina.

#### 4.3. The Thin RGB of Carina

The fact that Carina has a very narrow RGB is unexpected given the wide ranges in ages and metal abundances encom-

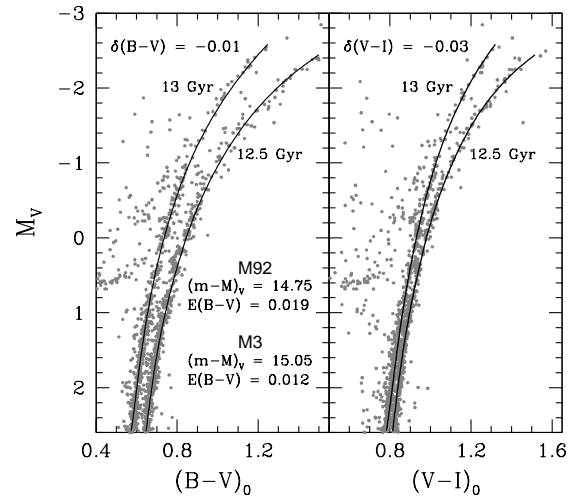


**Figure 10.** Fits of the RGB segments of 13.0 Gyr,  $[\text{Fe}/\text{H}] = -2.40$  and 12.5 Gyr,  $[\text{Fe}/\text{H}] = -1.55$  isochrones to the giant branches of M92 and M3, respectively. (M92 has a bluer RGB than M3.) Both isochrones assume  $Y = 0.25$  and  $[\alpha/\text{Fe}] = 0.40$  and both were adjusted by  $\delta(B-V) = -0.01$  and  $\delta(V-I) = -0.03$  mag in order to provide the best overall fits to the cluster observations.

passed by its stellar populations. As Venn et al. (2012) have remarked in their recent study of this dSph, it is possible that the giants “have a fortuitous alignment in the age-metallicity degeneracy, such that the older metal-poor stars overlie the metal-enhanced intermediate-age stars”. Although this overlap is undoubtedly happening, to what extent *does* the observed RGB constrain the properties of Carina’s stellar populations? In what follows, we will endeavor to answer this question using several of the same isochrones that seem to provide quite good fits to the TO and HB observations.

Fortunately, the predicted morphologies of current Victoria-Regina isochrones reproduce the shapes of GC giant branches very well when standard reddenings (from Schlafly & Finkbeiner 2011), distances based on ZAHB models that satisfy RR Lyrae constraints (see V13, V14b), and metallicities close to those derived by, e.g., Kraft & Ivans (2003) and Carretta et al. (2009a) are assumed. As shown in the left-hand panel of Figure 10, the isochrones for the same ages and chemical abundances that were fitted to the turnoff observations of M3 and M92 in § 3.1, on the assumption of the cluster properties that are given explicitly in Fig. 3, provide a close match to their RGB populations on the  $[(B-V)_0, M_V]$ -diagram. To accomplish this, the  $B-V$  colors from the CV14 transformations had to be corrected by just  $-0.01$  mag, independently of gravity and  $T_{\text{eff}}$ . The right-hand panel shows that equally good agreement can be obtained on the  $[(V-I)_0, M_V]$ -diagram; but in this case, the required color adjustment turns out to be  $\delta(V-I) = -0.03$  mag. (The origin of the small zero-point offsets is not known, but they can be reasonably attributed to small photometric errors or minor problems with, e.g., the CV14 color transformations, the model  $T_{\text{eff}}$  scale, and/or the assumed cluster properties.)

What is especially encouraging is that exactly the same  $\delta(B-V)$  and  $\delta(V-I)$  color offsets are needed for both M3 and M92, despite the difference of nearly 1 dex in their  $[\text{Fe}/\text{H}]$  values. This implies that models which are fitted to the giant branch of Carina should be trustworthy in an absolute sense if we simply apply the same color adjustments to them. In effect, we have calibrated the RGBs of the Victoria-Regina isochrones using M92 and M3. (As shown by V14a, these

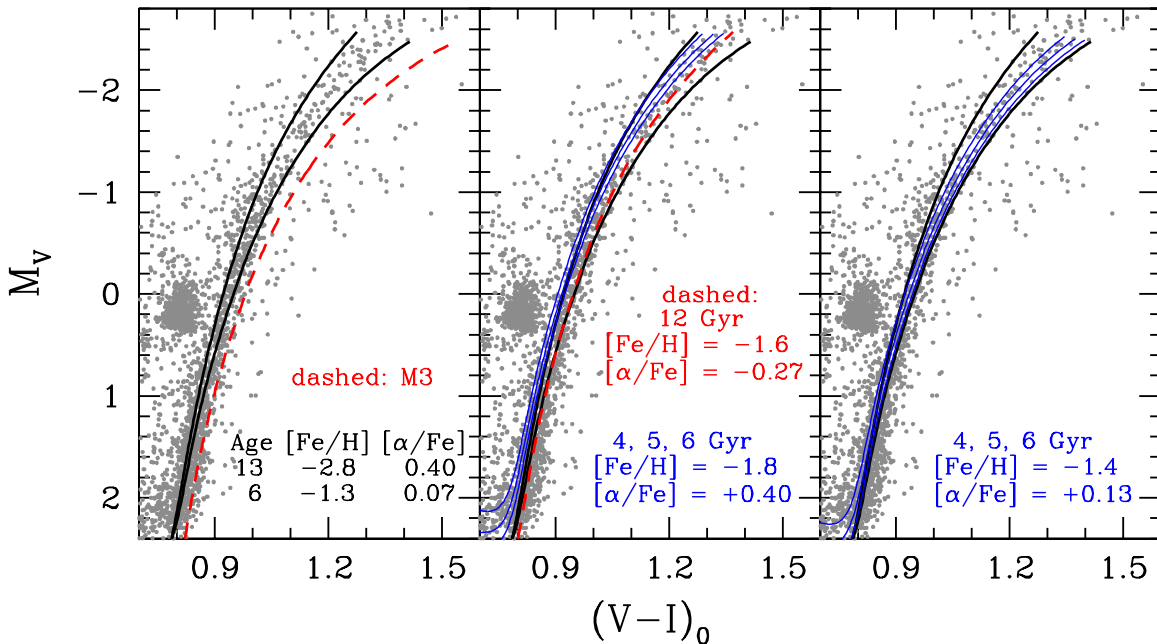


**Figure 11.** *Left-hand panel:* Overlay of the RGB portions of three isochrones onto the Carina CMD. The bluer of the two solid curves assumes  $[\text{Fe}/\text{H}] = -2.40$ ,  $[\alpha/\text{Fe}] = 0.40$ , and an age of 13 Gyr; the other one was generated for  $[\text{Fe}/\text{H}] = -1.30$ ,  $[\alpha/\text{Fe}] = 0.07$ , and an age of 6 Gyr. The dashed curve is the best-fit isochrone to the M3 RGB (see the previous figure). *Middle panel:* As in the left-hand panel, except that the dashed curve has the indicated properties and the thin solid curves represent the RGB portions of 4, 5, and 6 Gyr isochrones for  $[\text{Fe}/\text{H}] = -1.8$  and  $[\alpha/\text{Fe}] = 0.40$ . *Right-hand panel:* The same 6 and 13 Gyr isochrones that appear in the left-hand and middle panels have been replotted, along with three isochrones for the indicated ages and chemical properties (the thin solid curves). The adopted reddening and distance modulus of Carina are the same as in previous figures, and we have assumed that  $E(V-I) = 1.244E(B-V)$  (Casgrande & VandenBerg 2014). The predicted colors along the isochrones were adjusted by  $\delta(V-I) = -0.03$  mag prior to plotting them.

computations are equally successful over a much broader range in  $[\text{Fe}/\text{H}]$ . The main difficulty, as also reported by V13, is that somewhat different offsets are needed to fit the MSTO observations than to match the location of cluster RGBs; i.e., the predicted difference in color between the TO and the lower giant branch differs from the observed difference by a small amount. However, this is not of particular concern because, as noted at the end of the previous paragraph, such discrepancies could easily be due to relatively minor deficiencies in some of the more uncertain aspects of the stellar models, the assumed chemical compositions, etc.)

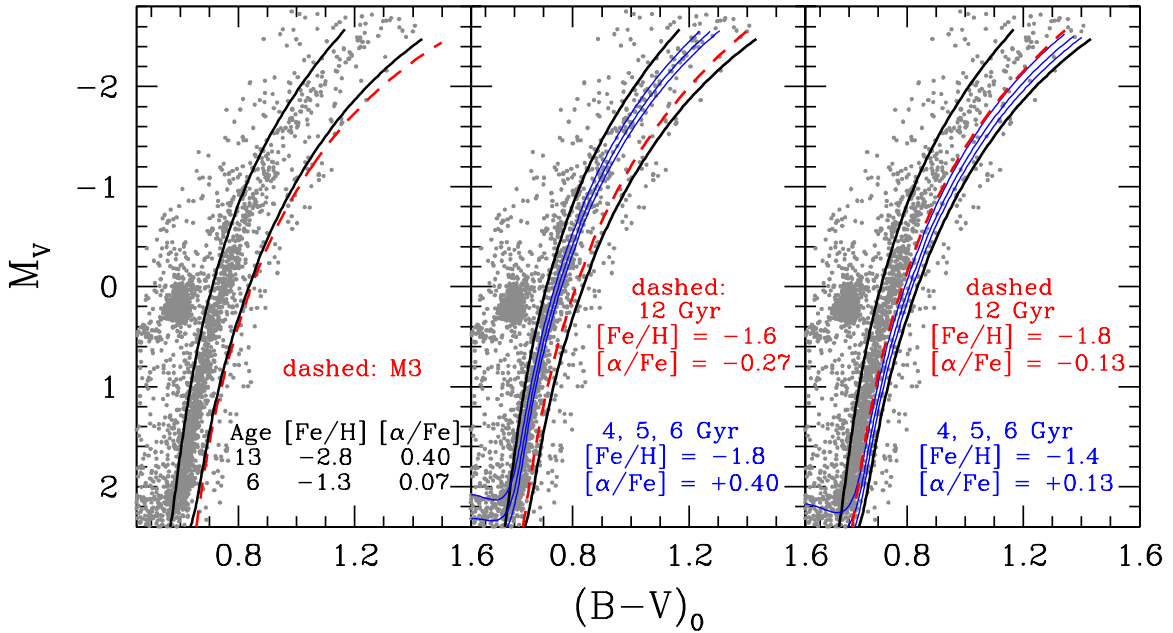
It is already apparent in Fig. 10 that a difference of 0.85 dex in  $[\text{Fe}/\text{H}]$  implies a much thinner RGB on the  $[(V-I)_0, M_V]$ -diagram, especially at  $M_V \gtrsim 0.0$ , than on the  $[(B-V)_0, M_V]$ -plane. This is the expected consequence of the fact that the  $B-V$  color index has a much stronger metallicity dependence than  $V-I$ . Because the latter will also be less affected by variations in the metals mixture, it should be more straightforward to interpret the fits of isochrones to the  $VI$  photometry of Carina than to CMDs based on  $BV$  data. Therefore, we will first examine the implications for the observed RGB on the  $[(V-I)_0, M_V]$ -diagram of the isochrones that have been compared with the TO observations in the previous section. ( $V-I$  colors were not considered previously because the brightness of the night sky in  $I$  makes it impossible to obtain ground-based photometry in this filter for the faintest TO stars in Carina.)

Figure 11 compares the giant branches of several isochrones with our  $VI$  data, assuming that Carina has  $E(B-V) = 0.054$  and  $(m-M)_V = 20.28$ , as adopted throughout this investigation. To deredden the  $V-I$  colors, we have assumed that  $E(V-I) = 1.244E(B-V)$  (see CV14). Since  $> 95\%$  of the stars in the dSph appear to have  $[\text{Fe}/\text{H}]$  values between  $-2.8$  and  $-1.3$  (according to the MDF in Fig. 1b), we have

plotted (in all three panels, as thick solid curves) the RGBs of a 13 Gyr isochrone for  $[\text{Fe}/\text{H}] = -2.8$ ,  $[\alpha/\text{Fe}] = +0.4$  and a 6 Gyr isochrone for  $[\text{Fe}/\text{H}] = -1.3$ ,  $[\alpha/\text{Fe}] = +0.07$  (consistent with the relation between  $[\alpha/\text{Fe}]$  and  $[\text{Fe}/\text{H}]$  shown in Fig. 1a). It is apparent (see the left-hand panel) that these isochrones bracket the upper-RGB populations quite well and that they predict an exceedingly thin lower RGB. The dashed curve represents the giant-branch segment of the the same isochrone that was superimposed on the CMD of M3 in Fig. 10. This is significantly redder than the majority of the bright giants in Carina, from which one would be inclined to conclude, in the absence of any additional information, that the galaxy has few, if any, stars with  $[\text{Fe}/\text{H}]$  values as high as  $-1.55$ . However, we know that from spectroscopic work that there are large numbers of giants with higher iron, but lower  $\alpha$ -element, abundances, and photometric studies have revealed the existence of many young stars. In accordance with standard stellar evolutionary theory (e.g., see V14a), the most iron-rich giants in Carina are bluer than the RGB of M3, at the same  $M_V$ , because the former are younger and  $\alpha$ -poor (in an absolute sense) relative to their cluster counterparts.<sup>7</sup>

In the middle panel of Fig. 11, a 12 Gyr isochrone for  $[\text{Fe}/\text{H}] = -1.6$  and  $[\alpha/\text{Fe}] = -0.27$  has been overlaid onto the Carina CMD, along with the same two isochrones from the left-hand panel (the thick solid curves) and 4–6 Gyr isochrones for  $[\text{Fe}/\text{H}] = -1.8$ ,  $[\alpha/\text{Fe}] = +0.4$  (the thin solid curves). The separation in color at a fixed magnitude between the old  $-2.8$  and  $-1.6$  isochrones is quite small — easily consistent with the observed spread in RGB colors at a given luminosity (at least on this CMD). Whereas the three isochrones for intermediate ages lie between those for  $[\text{Fe}/\text{H}] = -2.8$  and

<sup>7</sup> It should be kept in mind that it is the absolute abundances of the metals, not  $[m/\text{Fe}]$  ratios, that are important for stellar models.



**Figure 12.** As in the previous figure, except that the comparisons between theory and observations are made on the  $[(B-V)_0, M_V]$ -diagram and the isochrone colors were corrected by  $\delta(B-V) = -0.01$  mag.

$-1.3$  at  $M_V \lesssim -1$ , they are located slightly to the blue of the lowest metallicity isochrone at fainter absolute magnitudes. Even so, the width of the RGB below the HB clump is still very narrow, and it would remain so even if the range in  $[\text{Fe}/\text{H}]$  or age were expanded somewhat. In fact, the predicted RGB is actually a bit thinner than the observed one, which may be a consequence of photometric errors, small as they are (see § 2). Note that old ( $\sim 12$  Gyr) isochrones for  $[\text{Fe}/\text{H}] < -1.6$  would overlie the 4–6 Gyr isochrones that have been plotted for  $[\text{Fe}/\text{H}] = -1.8$ , which illustrates the well-known age-metallicity degeneracy.

Very similar comparisons between theory and observations are shown in the right-hand panel; in this case, the intermediate-age isochrones are for  $[\text{Fe}/\text{H}] = -1.4$  and  $[\alpha/\text{Fe}] = +0.13$ . Not unexpectedly, they lie just to the blue of the 6 Gyr isochrone for  $[\text{Fe}/\text{H}] = -1.3$  and  $[\alpha/\text{Fe}] = +0.07$ . A similar set of 4–6 isochrones was computed for  $[\text{Fe}/\text{H}] = -1.6$  and  $[\alpha/\text{Fe}] = +0.27$ , which is also consistent with the  $[\alpha/\text{Fe}]$  vs.  $[\text{Fe}/\text{H}]$  relation in Fig. 1a, and although we have chosen not to plot them here, they lie approximately midway between those for  $[\text{Fe}/\text{H}] = -1.8$  (middle panel) and  $-1.4$  (right-hand panel). As a result, they would overlie the densest concentration of Carina giants better than the latter, which is perhaps to be expected since the peak in the MDF occurs at  $[\text{Fe}/\text{H}] \sim -1.65$  (see Fig. 1b).

In hindsight, it is not too much of a surprise that the Carina RGB is very narrow on the  $[(V-I)_0, M_V]$ -diagram, given that the vast majority of its stars appear to be more metal-rich than M92, more metal-poor than M3 (largely due to the low abundances of the  $\alpha$ -elements), and older than  $\sim 3$  Gyr (see Fig. 5). Because nearly all of the giants in the dSph lie to the blue of M3’s RGB, (see the left-hand panel of Fig. 11), it is to be expected that the thickness of the galactic RGB will be less than the separation between the M92 and M3 giant branches, which amounts to only  $\delta(V-I) \approx 0.04$  mag at  $M_V$  values that are fainter than the cluster HBs (see Fig. 10). Young ( $< 3$  Gyr),  $[\text{Fe}/\text{H}] \lesssim -1.8$  Gyr giants would be located on the blue side of a 13 Gyr,  $[\text{Fe}/\text{H}] = -2.8$  isochrone, but they do not ap-

pear to be present, at least in significant numbers (see Fig. 11). We conclude that the thin RGB of Carina is completely consistent with the observed and derived properties of its stellar populations, even if moderately large uncertainties are taken into account.

However,  $V-I$  colors are a better discriminator of differences in  $T_{\text{eff}}$  than of metallicity, so it is instructive to perform the same comparisons of isochrones with the RGB of Carina as those just discussed, but on the  $[(B-V)_0, M_V]$ -diagram. Indeed, the analogous plot (see Figure 12) differs by more than one might have anticipated from the previous one, though there are several similarities as well. The most noticeable difference is that the giants are not as centrally located between the two thick solid curves as in Fig. 11 (compare the left-hand panels). Indeed, the 6 Gyr isochrone for  $[\text{Fe}/\text{H}] = -1.3$  and  $[\alpha/\text{Fe}] = +0.07$  is significantly redder than the red edge of the distribution of giants, though a much better fit to the latter is obtained by a 4 Gyr isochrone for the same metal abundances (judging from the location of the isochrone for  $[\text{Fe}/\text{H}] = -1.4$  and  $[\alpha/\text{Fe}] = +0.13$  in the right-hand panel). In addition, the median RGB of Carina seems to be matched quite well by 5–6 Gyr isochrones for  $[\text{Fe}/\text{H}] = -1.8$  and  $[\alpha/\text{Fe}] = +0.4$  (see the middle panel). Both of these isochrones were located just to the left of the main concentration of bright giants on the  $[(V-I)_0, M_V]$ -plane.

As found previously, a 13 Gyr isochrone for  $[\text{Fe}/\text{H}] = -2.8$  and  $[\alpha/\text{Fe}] = +0.4$  provides a good fit to the blue edge of the distribution of Carina giants. Why the same interpretation of the redder stars is not found from both  $B-V$  and  $V-I$  colors is not clear, but there are a few possible explanations for this. For one, it is possible that the  $[\text{Fe}/\text{H}]$  scale derived by Starkenburg et al. (2010), which has been assumed here (see Fig. 1b), is too metal-rich by  $\sim 0.15$ – $0.2$  dex. Such a shift, which is  $\lesssim$  the differences in measured GC metallicities over the years (e.g., see Carretta & Gratton 1997, Kraft & Ivans 2003, Carretta et al. 2009a) would affect the horizontal separation between the two isochrones in the left-hand panel of Fig. 12 considerably more than in the case of the

corresponding isochrones in Fig. 11.<sup>8</sup> We see, for instance, that a 12 Gyr isochrone for  $[\text{Fe}/\text{H}] = -1.8$  provides a much better fit to the red edge of the main distribution of Carina giants (right-hand panel) than the 12 Gyr isochrone for  $[\text{Fe}/\text{H}] = -1.6$  that has been plotted in the middle panel. (If it is only the iron abundance that changes, the derived value of  $[\alpha/\text{Fe}]$  would increase by the amount that the value of  $[\text{Fe}/\text{H}]$  is reduced. However, one could compensate for that by decreasing the assumed age. For example, a 10 Gyr isochrone for  $[\text{Fe}/\text{H}] = -1.8$  and  $[\alpha/\text{Fe}] = +0.02$  is essentially indistinguishable from one for the same  $[\text{Fe}/\text{H}]$ , but  $[\alpha/\text{Fe}] = -0.13$ ; see the right hand panel.)

This brings us to the second possibility, which is that stars of different metal abundances have different ages (as suggested by our simulations in the case of the oldest stars). Fig. 12 shows that a 6 Gyr isochrone for  $[\text{Fe}/\text{H}] = -1.8$  and  $[\alpha/\text{Fe}] = +0.4$  (middle panel) is bluer than a 4 Gyr isochrone for  $[\text{Fe}/\text{H}] = -1.4$  and  $[\alpha/\text{Fe}] = +0.13$  (right-hand panel) by only a small amount. In fact, the latter would be nearly coincident with the former if it had an age of 3 Gyr. (This explanation would indeed imply that ages vary with metallicity in just the right way to produce a thin giant branch.) In addition, variations in the heavy-element mixture may explain some of the differences in the fits of isochrones to the  $BV$  and  $VI$  photometry of Carina giants. It is an approximation to adopt the same abundances for all of the  $\alpha$ -elements at a given  $[\text{Fe}/\text{H}]$  value. As shown by V12, the location of the RGB on the theoretical plane has a comparable dependence on the abundance of Si as of Mg, and if, e.g.,  $[\text{Si}/\text{Fe}] < [\text{Mg}/\text{Fe}]$ , then the values of  $[\alpha/\text{Fe}]$  that we have assumed are too high, and the isochrones (especially at higher metallicities) are too red. Unfortunately, not a great deal is known about the abundances of silicon in Carina. (Star-to-star abundance variations will also have important consequences for stellar temperatures and colors, but color transformations that allow for differences in the abundances of single elements are not yet available.) At this stage, the uncertainties are still large enough that the minor inconsistencies that exist between Figs. 11 and 12 are not of particular concern.

## 5. SUMMARY

The most important result of this investigation is that stellar models are able to reproduce the main features of the CMD of Carina quite well when they assume the full range in metal abundances ( $\gtrsim 1.5$  dex in  $[\text{Fe}/\text{H}]$ ) that has been derived from high-quality spectroscopic data. This contradicts previous findings, notably by Bono et al. (2010), who argued from their analysis of the observed photometry that the metallicity variations encompassed by either the oldest or intermediate-age populations cannot amount to much more than a few tenths of a dex. The key to our success is that we have used isochrones (from V14a) which assume heavy-element abundances that follow the observed relations between  $[\alpha/\text{Fe}]$  and  $[\text{Fe}/\text{H}]$ . (Interpolations in those grids can be made for any value of  $[\alpha/\text{Fe}]$  between  $-0.4$  and  $+0.4$  at a fixed  $[\text{Fe}/\text{H}]$  value.) In fact, it would not have been possible to reproduce some CMD features, such as the small range in luminosity spanned by the

<sup>8</sup> If anything, spectroscopic studies in the past few years have caused even more consternation regarding *absolute*  $[\text{Fe}/\text{H}]$  determinations than earlier ones. For instance, whereas Carretta et al. (2009a) found that M15, M92, and NGC 5466 all have  $[\text{Fe}/\text{H}]$  values within the range of  $-2.31$  to  $-2.35$ , Sobeck et al. (2011) and Roederer & Sneden (2011) have obtained  $[\text{Fe}/\text{H}] \lesssim -2.6$  for M15 and M92, respectively, while Lamb et al. (2015) have derived a value of  $-1.97$  for NGC 5466.

old HB component of Carina, using models for the measured range in  $[\text{Fe}/\text{H}]$  *unless*  $[\alpha/\text{Fe}]$  is a strongly decreasing function of the iron abundance (as observed). In other words, models for constant  $[\alpha/\text{Fe}]$ , irrespective of the value that is adopted, are incapable of providing a satisfactory explanation of the Carina CMD.

Being able to transform our models to the  $[(B-V)_0, M_V]$ - and  $[(V-I)_0, M_V]$ -diagrams using fully consistent transformations (from CV14) has certainly made a difference as well, because predicted  $BVI$  magnitudes have a considerable dependence on the abundances of the  $\alpha$ -elements at fixed values of  $[\text{Fe}/\text{H}]$ ,  $\log g$ , and  $T_{\text{eff}}$ . Furthermore, we have taken the additional step of determining, and applying, corrections to the CV14  $(B-V)-T_{\text{eff}}$  relations in order that isochrones reproduce the CMDs of M3 and M92, when very good estimates of their reddening, metallicities, and distances are assumed. This ‘‘calibration’’ of the isochrones ensures that the models faithfully reproduce the locations of the MSTOs and lower RGBs, as well as the slopes of the SGBs in GCs that span a range of nearly 1 dex in  $[\text{Fe}/\text{H}]$ , thereby giving us confidence that they will accurately represent the properties of stars in the dSph. This procedure should minimize errors that would otherwise be present, and possibly be quite substantial.

The veracity of this assertion is easily verified. There is a general tendency of Victoria-Regina isochrones to suffer from small zero-point and systematic offsets when compared with GC CMDs, though the predicted slopes of the MS and RGB look fine (see, e.g., the plots provided by V13 and V14a). When compared with the same *HST* observations that were the subject of the paper by V13, Dartmouth isochrones appear to be considerably more problematic (see Dotter et al. 2010; the right-hand panels of their Figs. 4 and 5). Differences in the color transformations that were employed in the respective studies are likely to be mostly responsible for this, in view of the fact that very similar physics has been incorporated in both the Victoria and Dartmouth codes. However, the same cannot be said of BASTI isochrones (e.g., Pietrinferni et al. 2004) because these computations do not take diffusive processes into account, which have significant consequences for turnoff luminosity versus age relations and the predicted  $T_{\text{eff}}$  scale, especially at low metallicities and high ages (see VandenBerg et al. 2002; their Fig. 2).

It is risky to use stellar models from *any* source without carefully examining how well they satisfy empirical constraints. This is especially true when attempting to interpret the photometry of a galaxy, like Carina. When an isochrone is overlaid onto the observed CMD, it should superimpose stars of nearly the same age and chemical abundances whether they are located near the TO, along the SGB, or on the giant branch. This is, of course, complicated by known degeneracies between the effects of age and chemical abundances, but if the adopted isochrones do not reproduce the locations and morphologies of GC CMDs particularly well, those models are unlikely to provide very meaningful results when applied to galactic observations. (GC ages, in contrast, mainly involve fits of isochrones to turnoff stars.)

The ages of the different stellar populations in Carina that we obtained from overlays of isochrones onto the observed CMD are quite similar to those found previously, especially in a relative sense. The oldest of the intermediate-age stars appear to have formed 6–6.5 Gyr ago, whereas the range in age needed to reconcile stellar models with the faintest turnoff/SGB stars is  $\sim 9$ –14 Gyr. In agreement with earlier determinations, there was apparently a  $\sim 3$ –4 Gyr hiatus in

the formation of stars in Carina after the first SF epoch.

Our CMD simulations, which are based on isochrones that have been carefully calibrated, rule out the possibility that the faintest TO/SGB stars in Carina are a single-age population by more than  $6\sigma$ . However, simulations in which ages are limited to the range 8–14.4 Gyr and iron abundances to  $-3.0 \leq [\text{Fe}/\text{H}] \leq -1.4$ , without constraining how the number of stars varies with metallicity, provide a significantly better match to the observed CMD if the earliest star formation epoch lasted a few Gyr. Moreover, judging from the derived weighting of the points in a grid of age and  $[\text{Fe}/\text{H}]$ , there are two ways of obtaining a reasonable approximation to the observed MDF (both of which suggest that ages decrease somewhat with increasing  $[\text{Fe}/\text{H}]$ ). Either the adopted distance modulus,  $(m-M)_V = 20.28$ , should be increased by  $\sim 0.1$  mag, if  $[\alpha/\text{Fe}]$  varies with  $[\text{Fe}/\text{H}]$  according to the relation shown in Fig. 1a, or the assumed O abundances should be increased and the dependence of  $[\text{O}/\text{H}]$  on  $[\text{Fe}/\text{H}]$  is similar to that adopted by Brown et al. (2014). In support of the latter possibility, we note that  $[\text{O}/\text{Fe}] \gtrsim +0.6$  is typically found in very metal poor, Galactic halo stars (e.g., García Pérez et al. 2006, Ramírez et al. 2012), and as discussed in § 4.1, it may be difficult to reconcile the distribution of stars along the old HB component of Carina with the observed MDF unless the stars have relatively high O abundances. (A larger distance seems unlikely in view of the recent empirical determinations by Pietrzyński et al. 2009 and Coppola et al. 2013.)

Although our isochrones had no difficulty reproducing the narrow RGB of Carina on the  $V-I, V$  CMD, the observed width on the  $B-V, V$  color plane was found to be smaller than expected. Improved consistency would be obtained if the age-metallicity relations that describe the stellar populations in Carina have significant slopes, in the expected sense that more metal-rich stars are younger. In fact, this is suggested by the simulations that we, and de Boer et al. (2014b), have carried out for the oldest, and intermediate-age, populations of Carina, respectively. (Our simulations were limited to the oldest stars because extensions of the V14a grids to younger ages are not available.) In addition, or alternatively, this difficulty may be a reflection of current uncertainties associated with the observed  $[\text{Fe}/\text{H}]$  scale, the assumed  $[\alpha/\text{Fe}]$  values (which are based entirely on Mg, as little is known about the abundances of Si), and/or the color transformations. While a resolution of this problem must be left for future work, it is very encouraging that modern stellar models, on the assumption of the chemical abundances which have been derived from high-resolution spectroscopy, are able to explain most of the features of Carina's CMD quite well.

We thank both Chris Pritchett, who pointed out a very useful reference, and Kim Venn for helpful discussions. D.A.V acknowledges the support of a Discovery Grant from the Natural Sciences and Engineering Research Council of Canada.

#### REFERENCES

- Battaglia, G., Irwin, M. J., Tolstoy, E., de Boer, T., & Mateo, M. 2012, *ApJ*, 761, L31
- Bono, G., Stetson, P. B., Walker, A. R., et al. 2010, *PASP*, 122, 651
- Brown, T. M., Smith, E., Ferguson, H. C., et al. 2006, *ApJ*, 652, 323
- Brown, T. M., Tumlinson, J., Geha, M., et al. 2012, *ApJ*, 735, L21
- Brown, T. M., Tumlinson, J., Geha, M., et al. 2014, *ApJ*, 796, 91
- Carretta, E., Bragaglia, A., Gratton, R. G., D'Orazi, V., & Lucatello, S. 2009a, *A&A*, 508, 695
- Carretta, E., Bragaglia, A., Gratton, R. G., & Lucatello, S. 2009b, *A&A*, 505, 139
- Carretta, E., & Gratton, R. G. 1997, *A&AS*, 121, 95
- Casagrande, L., & VandenBerg, D. A. 2014, *MNRAS*, 444, 392 (CV14)
- Castellani, V., & Degl'Innocenti, S. 1995, *A&A*, 298, 827
- Cayrel, R., Depagne, E., Spite, M., et al. 2004, *A&A*, 416, 1117
- Coppola, G., Stetson, P. B., Marconi, M., et al. 2013, *ApJ*, 775, 6
- de Boer, T. J. L., Belokurov, V., Beers, T. C., & Lee, Y. S. 2014a, *MNRAS*, 443, 658
- de Boer, T. J. L., Tolstoy, E., Lemasle, B., Saha, A., Olszewski, E. W., Mateo, M., Irwin, M. J., & Battaglia, G. 2014b, *A&A*, 572, A10
- Dolphin, A. E. 2002, *MNRAS*, 332, 91
- Dotter, A., Sarajedini, A., Anderson, J., et al. 2010, *ApJ*, 708, 698
- Fabbian, D., Nissen, P. E., Asplund, M., Pettini, M., & Akerman, C. 2009, *A&A*, 500, 1143
- Fabrizio, M., Merle, T., Thévenin, F., et al. 2012, *PASP*, 124, 519
- Frebel, A. 2010, *AN*, 331, 474
- García Pérez, A. E., Asplund, M., Primas, F., Nissen, P. E., & Gustafsson, B. 2006, *A&A* 451, 621
- Gilmore, G. F., & Wyse, R. F. G. 1991, *ApJ*, 367, L55
- Gilmore, G. F., & Wyse, R. F. G. 1998, *AJ*, 116, 748
- Harris, J., & Zaritsky, D. 2001, *ApJS*, 136, 25
- Hurley-Keller, D., Mateo, M., & Nemeč, J. 1998, *AJ*, 115, 1840
- Kirby, E. N., Cohen, J. G., Smith, G. H., Majewski, S. R., Sohn, S. T., & Guhathakurta, P. 2011, *ApJ*, 727, 79
- Koch, A., Grebel, E. K., Wyse, R. F. G., et al. 2006, *AJ*, 131, 895
- Koch, A., Grebel, E. K., Gilmore, G. F., et al. 2008, *AJ*, 135, 1580
- Komatsu, E., Smith, K. M., Dunkley, J., et al. 2011, *ApJS*, 192, 18
- Kraft, R. P., & Ivans, I. I. 2003, *PASP*, 115, 143
- Lamb, M. P., Venn, K. A., Shetrone, M. D., Sakari, C. M., & Pritzl, B. J. 2015, *MNRAS*, 448, 42
- Landolt, A. 1973, *AJ*, 78, 959
- Landolt, A. 1992, *AJ*, 104, 340
- Lemasle, B., Hill, V., Tolstoy, E., et al. 2012, *A&A*, 538, A100
- Lianou, S., Grebel, E. K., & Koch, A. 2011, *A&A*, 531, A152
- Maoz, D., Mannucci, F., & Nelemans, G. 2014, *ARA&A*, 52, 107
- McWilliam, A. 1997, *ARA&A*, 35, 503
- Minor, Q. E. 2013, *ApJ*, 779, 116
- Monelli, M., Milone, A. P., Fabrizio, M., et al. 2014, *ApJ*, 796, 90
- Pietrinferni, A., Cassisi, S., Salaris, M., & Castelli F. 2004, *ApJ*, 612, 168
- Pietrzyński, G., Górski, M., Gieren, W., Ivanov, V. D., Bresolin, F., & Kudritzki, R.-P. 2009, *AJ*, 138, 459
- Ramírez, I., Meléndez, J., & Chanamé, J. 2012, *ApJ*, 757, 164
- Roederer, I. U., & Sneden, C. 2011, *AJ*, 142, 22
- Sarajedini, A., Bedin, L. R., Chaboyer, B., et al. 2007, *AJ* 133, 1658
- Schlafly, E. F., & Finkbeiner, D. P. 2011, *ApJ*, 737, 103
- Shetrone, M. D., Venn, K. A., Tolstoy, E., Primas, F., Hill, V., & Kaufer, A. 2003, *AJ*, 125, 684
- Smecker-Hane, T. A., Stetson, P. B., Hesser, J. E., & Lehnert, M. D. 1994, *AJ*, 108, 507
- Sobeck, J. A., Kraft, R. P., Sneden, C., et al. 2011, *AJ*, 141, 175
- Starkenbourg, E., Hill, V., Tolstoy, E., et al. 2010, *A&A*, 513, A34
- Stetson, P. B. 2000, *PASP*, 112, 925
- Stetson, P. B. 2005, *PASP*, 117, 563
- VandenBerg, D. A., & Bell, R. A. 2001, *New Astr. Rev.*, 45, 577
- VandenBerg, D. A., Bergbusch, P. A., Dotter, A., Ferguson, J. W., Michaud, G., Richer, J., & Proffitt, C. R. 2012, *ApJ*, 755, 15 (V12)
- VandenBerg, D. A., Bergbusch, P. A., Ferguson, J. W., & Edvardsson, B. 2014a, *ApJ*, 794, 72 (V14a)
- VandenBerg, D. A., Bond, H. E., Nelan, E. P., Nissen, P. E., Schaefer, G. H., & Harmer, D. 2014b, *ApJ*, 792, 110 (V14b)
- VandenBerg, D. A., Brogaard, K., Leaman, R., & Casagrande, L. 2013, *ApJ*, 775, 134 (V13)
- VandenBerg, D. A., & Clem, J. L. 2003, *AJ*, 126, 778
- VandenBerg, D. A., Richard, O., Michaud, G., & Richer, J. 2002, *ApJ*, 571, 487
- VandenBerg, D. A., Swenson, F. J., Rogers, F. J., Iglesias, C. A., & Alexander, D. R. 2000, *ApJ*, 532, 430
- Venn, K. A., Irwin, M., Shetrone, M. D., Tout, C. A., Hill, V., & Tolstoy, E. 2004, *AJ*, 128, 1177
- Venn, K. A., Shetrone, M. D., Irwin, M. J., et al. 2012, *ApJ*, 751, 102
- Vivas, A. K., & Mateo, M. 2013, *AJ*, 146, 141